Published for SISSA by Springer

Received: April 4, 2025
Accepted: April 23, 2025
Published: June 26, 2025

Beautiful Majorana Higgses at colliders

Benjamin Fuks[a], **Jonathan Kriewald**[b], **Miha Nemevšek**[b,c] **and Fabrizio Nesti**[d,e]

[a] *Laboratoire de Physique Théorique et Hautes Energies (LPTHE), UMR 7589, Sorbonne Université & CNRS, 4 place Jussieu, 75252 Paris Cedex 05, France*
[b] *Jožef Stefan Institute, Jamova 39, 1000 Ljubljana, Slovenia*
[c] *Faculty of Mathematics and Physics, University of Ljubljana, Jadranska 19, 1000 Ljubljana, Slovenia*
[d] *Dipartimento di Scienze Fisiche e Chimiche, Università dell'Aquila, via Vetoio, I-67100, L'Aquila, Italy*
[e] *INFN, Laboratori Nazionali del Gran Sasso, I-67100 Assergi (AQ), Italy*

E-mail: fuks@lpthe.jussieu.fr, jonathan.kriewald@ijs.si, miha.nemevsek@ijs.si, fabrizio.nesti@aquila.infn.it

Abstract: We investigate a novel collider signature within the minimal Left-Right Symmetric Model, featuring a Higgs sector composed of a bi-doublet and two triplets. Our study focuses on a region of the parameter space where the $\mathrm{SU}(2)_R$ charged gauge boson W_R lies in the multi-TeV regime (3–100 TeV) and the additional Higgs states play a significant role. In this scenario, a heavy neutral Higgs boson Δ with a dominant $\mathrm{SU}(2)_R$ triplet component can be produced in association with either a Standard Model Higgs boson or a massive weak boson. The subsequent decay of the heavy Higgs into Majorana neutrinos N results in displaced lepton signatures, providing a striking manifestation of lepton number violation. Additionally, we explore how the production of b-jets in these processes can enhance hadron-collider sensitivity to such signals. A particularly compelling channel, $pp \to b\bar{b}NN$, offers the exciting possibility of simultaneously probing the spontaneous mass origin of both Dirac fermions and Majorana states. Based on an optimised event selection strategy and state-of-the-art Monte Carlo simulations, we outline the expected reach at the HL-LHC and future colliders. Our findings demonstrate that this channel probes a region of parameter space where the neutral Higgs triplet and heavy neutrino masses are relatively light ($m_\Delta \lesssim 250$ GeV, $m_N \lesssim 80$ GeV), indirectly constraining the W_R boson to the deep multi-TeV domain, with sensitivity extending up to 70–80 TeV, effectively turning the LHC into a precision machine.

Keywords: Baryon/Lepton Number Violation, Left-Right Models, New Gauge Interactions

ArXiv ePrint: 2503.21354

Open Access, © The Authors.
Article funded by SCOAP[3].

https://doi.org/10.1007/JHEP06(2025)254

JHEP06(2025)254

Contents

1 Introduction **1**

2 The minimal left-right symmetric model **4**

3 Pair and associated production of Δ at pp colliders **6**
3.1 The Δ-strahlung process, $pp \to V^* \to V\Delta$ 7
3.2 Heavy Higgs production via gluon fusion 8
3.3 Cross sections for Δ production at proton-proton colliders 10

4 Heavy Higgs and neutrino decays and branching ratios **11**
4.1 Δ decays 11
4.2 Right-handed neutrino decay and lifetime 13

5 Sensitivities at run-3 and HL-LHC **17**
5.1 Displaced Majorana Higgses 17
5.2 The $b\bar{b}NN$ signature 21

6 Conclusion and outlook **23**

A Box amplitudes for $gg \to S_1 S_2$ **24**

B Phase space integration **26**

C Efficiency tables **27**

1 Introduction

Explaining the origin of neutrino mass remains one of the most significant mysteries still left unresolved by the Standard Model (SM) of particle physics. Perhaps the most elegant way of accounting for neutrino masses is the seesaw mechanism [1–5] that postulates the existence of new degrees of freedom, leading to light Majorana neutrinos. Another aesthetic puzzle of the SM is the complete asymmetry of weak interactions that couple chirally to left-handed components only via the $\mathrm{SU}(2)_L$ gauge group. Within the minimal Left-Right [4, 6, 7] symmetric model (LRSM), these two problems are resolved simultaneously by extending the gauge group to $\mathrm{SU}(2)_L \times \mathrm{SU}(2)_R \times \mathrm{U}(1)_{B-L}$. The $\mathrm{SU}(2)_R$ gauge group gets spontaneously broken [8] at a scale v_R, which is necessarily above the electroweak scale and at least within a few TeVs. The model enjoys an additional discrete Left-Right (LR) exchange symmetry, either in the form of $\mathcal{P}$ or $\mathcal{C}$ conjugation [9], that is broken together with the $\mathrm{SU}(2)_L \times \mathrm{SU}(2)_R \times \mathrm{U}(1)_{B-L}$ symmetry. This gauge symmetry moreover necessarily requires three generations of right-handed neutrinos that may obtain a Majorana mass when the symmetry is broken by the vacuum expectation values (vevs) of a pair of scalar triplets $\Delta_{L,R}$ and a single scalar bi-doublet ϕ.

JHEP06(2025)254

Imposition of either LR discrete symmetry in the Yukawa sector severely restricts the flavour structure of the LRSM, effectively requiring the right-handed quark mixing to be (nearly) equal to the CKM matrix for the case of $(\mathcal{P})$ $\mathcal{C}$ conjugation. This leads to strong flavour constraints [10], mainly from kaon mixing, which push v_R in the few TeV regime and the bi-doublets mass scale even higher [11]. These studies have been continuously updated [9, 12, 13], taking into account CP-violating constraints, electric dipole moments [14–17] and addressing the strong CP problem [16, 18, 19]. The bottom-line is that even though the flavour constraints impose the typical LRSM mass scale to lie deep in the TeV region, collider searches are competitive and may constitute the first evidence of new physics stemming from the LR symmetry. One may also contemplate how to explain dark matter [20, 21], which is an attractive possibility, however due to dilution constraints [22] the LR scale needs in this case to be far above the TeV scale [23, 24].

In the LRSM there are two sources of neutrino mass [25], a first one originating from Dirac mass terms and the right-handed Majorana mass terms (through a so-called type I seesaw), and another one directly connected to the vev of the $\mathrm{SU}(2)_L$ Higgs triplet (type II). Because of the LR symmetry, the two Dirac and Majorana mass sources are strongly related [26], and the heavy-light neutrino mixing can thus be determined in a closed form using the Cayley-Hamilton formula [27]. Ultimately, we would like to directly probe the full microscopic origin of neutrino masses by observing and separating the channels that depend on Majorana and Dirac couplings. In the SM [28], this is straightforward: the Higgs boson h decays to an $f\bar{f}$ fermion-antifermion pair with a rate $\Gamma(h \to f\overline{f}) \propto m_f^2$ (with m_f referring to the mass of the fermion f). This has been confirmed experimentally at least for the b quark and the tau lepton, and indirectly for the top quark and through an upper bound for the muon [29, 30]. In the LRSM, the right-handed neutrinos N get their Majorana mass from the spontaneous breaking of $\mathrm{SU}(2)_R$. This is reflected in the rate $\Gamma(\Delta \to NN) \propto m_N^2$ (where $\Delta \equiv \Delta_R^0$ stands for the neutral component of the $\mathrm{SU}(2)_R$ Higgs triplet and m_N for the heavy neutrino mass), a relation that should be tested directly in data. A handle on this challenge resides in the fact that the SM Higgs boson h and LRSM Δ boson mix. This has two consequences: firstly it becomes possible to probe the spontaneous origin of the mass of the heavy neutrino N via the $h \to NN$ decay [31], and secondly the $\mathrm{SU}(2)_R$ Higgs triplet can be produced via gluon fusion, thus offering a direct access to a 'Majorana Higgs' signature $gg \to \Delta \to NN$ [32]. In this work, we study further such opportunities offered within the LRSM to probe neutrino mass generation.

The Higgs sector of the LRSM has been studied to various degrees of detail, from the original spontaneous LR symmetry breaking mechanism [8, 33], to the more complete treatment of the scalar mass matrices [34–38] and determination of the constraints originating from electroweak observables and perturbativity [39–41]. Recently [27], we revisited this issue, diagonalised analytically the mass matrices and thus devised a physical input scheme with masses and mixing angles. This was then implemented through a FeynRules [42, 43]/UFO [44, 45] model file enabling state-of-the-art Monte Carlo simulations at next-to-leading-order (NLO) in QCD and leading-order loop-induced processes, that we heavily use in the present work.

A number of searches at high energy colliders have investigated LRSM signatures in different regions of the parameter space, and with qualitatively different final states. Perhaps

JHEP06(2025)254

the most model-independent limit comes from searches with di-jet [46, 47] and tb [48, 49] final states, since the left-handed and right-handed CKM matrices are similar [9, 12, 50, 51]. As soon as at least one right-handed neutrino is below the W_R mass threshold, it can be efficiently produced through the Keung-Senjanović (KS) [52] channel that may signal lepton-number violations if the final state particles are well separated in the transverse plane. This could exploit both the process $pp \to W_R^\pm \to \ell^\pm N \to \ell^\pm \ell^\pm jj$ where light jets are produced, and the process $pp \to W_R^\pm \to \ell^\pm N \to \ell^\pm \ell^\pm tb$ where a top-antibottom or an antitop-bottom pair is produced [53]. On the other hand, lowering the mass m_N of the heavy neutrino [54] results in merged non-isolated neutrino jets [55] that additionally become displaced before finally transitioning into a charged lepton and missing energy [56]. The latter signature can be efficiently constrained by recasting the bounds stemming from direct $W' \to \ell\nu$ searches [57–59], which yields the most significant direct bound on the mass of the W_R boson M_{W_R}. Obviously, the W_R boson can be deeply off-shell and new physics signals could still be observed away from the resonance [60]. Currently, the most sensitive bounds hence range in the $5 - 6\,\text{TeV}$ region, depending on the flavour of the final state charged lepton and on the value of m_N. Finally, it has been shown that future colliders have the potential to push these limits beyond 30 TeV [61].

While the gauge sector of the model has been quite thoroughly investigated, including the effects of gauge boson mixing [62] and Dirac masses [63–66], the Higgs sector still offers opportunities. In the minimal LRSM, flavour constraints push the bi-doublet in the $\mathcal{O}(20)$ TeV range, beyond the reach of the LHC [13, 17] and the left-handed triplet also needs to be heavy if the W_R boson is light [39]. The $\text{SU}(2)_R$ scalar triplet on the other hand contains a singly-charged Δ_R^+ state, which is the mostly would-be-Goldstone eaten by the W_R state, while its doubly-charged counterpart Δ_R^{++} and neutral component Δ are arbitrarily split and may be light, even lying around the TeV scale. As a result, the mixing between the h and Δ scalars can be significant, and this 'Majorana Higgs' scenario can be probed both in the $gg \to h \to NN$ [31] and $gg \to \Delta \to NN$ channels [32]. In this work we extend the analysis of [32], and consider not only the gluon fusion production mode, but also the associated channels $pp \to \Delta X$ with $X = W, Z, h$. The last process is particularly interesting from the conceptual point of view, because it offers a simultaneous handle on the Dirac mass origin of the bottom quarks originating from the SM Higgs decay, and the Majorana nature of the heavy neutrinos N stemming from the Δ decay. It thus manifestly signals lepton-number violation when $N \to \ell jj$ so that the final state comprises two same-sign or opposite-sign charged leptons and two b-jets, i.e. an exciting novel smoking gun signature of the LRSM. In this study, we consider the associated production process $pp \to \Delta h$, followed by the subsequent (and sometimes dominant) decays $h \to b\bar{b}$ and $\Delta \to NN$. This hence leads to a 'beautiful' Majorana final state with two b-jets and a pair of heavy neutrinos. The heavy neutrinos then decay as $N \to \ell^\pm jj$ into charged leptons and jets, producing a manifestly lepton-number violating final state. In addition, the heavy neutrino N can be significantly long-lived, decaying either inside the tracker, the muon chambers or even outside of a typical LHC detector. With enough luminosity, these fairly soft final state objects can thus be used to probe very high W_R boson mass values, extending well above the direct reach of the LHC.

We organise our discussion in the following way. First we summarise the relevant features of the LRSM in section 2, pointing out the set of input parameters for our analysis, the

JHEP06(2025)254

relevant couplings and their role in generating the signals considered. The phenomenological core of the paper lies in the following three sections, where we discuss Δ production in section 3 and (displaced) decays and branching ratios in section 4, before providing details on our collider analysis and the resulting sensitivities in section 5. In section 6 we conclude and provide some future outlook.

2 The minimal left-right symmetric model

The left-right symmetric model is a gauge extension of the SM based on the group

$$\mathcal{G}_{\rm LR} = \mathrm{SU}(3)_c \otimes \mathrm{SU}(2)_L \otimes \mathrm{SU}(2)_R \otimes \mathrm{U}(1)_{B-L}\,. \tag{2.1}$$

The whole model additionally enjoys a discrete LR-symmetry which exchanges the SU(2) gauge group factors and acts on the fermionic and scalar fields as a generalised parity $\mathcal{P}$ or charge conjugation $\mathcal{C}$. In addition to the usual left-handed fermion doublets $Q_L = (u_L, d_L)^T$ and $L_L = (\nu_L, \ell_L)^T$, the right-handed fermions are promoted to right-handed doublets $Q_R = (u_R, d_R)^T$ and $L_R = (\nu_R, \ell_R)^T$, including thus three right-handed neutral leptons ν_R. Due to the introduction of right-handed neutrinos ν_R, the gauge anomalies usually appearing due to the presence of the $\mathrm{U}(1)_{B-L}$ symmetry are conveniently cancelled, and the electric charge is defined as $Q = T_L^3 + T_R^3 + \frac{B-L}{2}$. The scalar sector of the LRSM comprises a bi-doublet field ϕ transforming as $(1,2,2,0)$ under the gauge group, and two (complex) scalar triplets $\Delta_{L,R}$ respectively transforming as $(1,3,1,2)$ and $(1,1,3,2)$,

$$\phi = \begin{pmatrix} \phi_1^{0*} & \phi_2^+ \\ \phi_1^- & \phi_2^0 \end{pmatrix}, \qquad \Delta_{L,R} = \begin{pmatrix} \frac{\Delta^+}{\sqrt{2}} & \Delta^{++} \\ \Delta^0 & -\frac{\Delta^+}{\sqrt{2}} \end{pmatrix}_{L,R}. \tag{2.2}$$

After the simultaneous spontaneous symmetry breaking of $\mathcal{G}_{\rm LR} \to \mathrm{SU}(3)_c \otimes \mathrm{U}(1)_{\rm em}$ symmetry group and of the discrete LR-symmetry, the model predicts the vacuum structure,

$$\langle\phi\rangle = \begin{pmatrix} v_1 & 0 \\ 0 & -e^{-i\alpha}v_2 \end{pmatrix}, \qquad \langle\Delta_{L,R}\rangle = \begin{pmatrix} 0 & 0 \\ v_{L,R} & 0 \end{pmatrix}, \tag{2.3}$$

with

$$v^2 = v_1^2 + v_2^2 \approx v_{\rm SM}^2\,, \qquad 0 \le \tan\beta = \frac{v_2}{v_1} \le 1\,. \tag{2.4}$$

In this case, $v_L \ll v \ll v_R$ and $v = 174\,\mathrm{GeV}$. The masses of the new heavy gauge bosons $W_R^\pm$ and Z_R are then approximately given by

$$M_{W_R} \simeq g v_R\,, \qquad M_{Z_R} \simeq \sqrt{3}\, M_{W_R}\,. \tag{2.5}$$

These two relations are valid up to $\mathcal{O}(v/v_R)$ corrections, and only when considering that parity is broken at low scales such that the $\mathrm{SU}(2)_L$ and $\mathrm{SU}(2)_R$ gauge couplings are equal $g_L = g_R \equiv g$. The resulting mixing between the heavy and light charged gauge bosons, driven by $\tan\beta$, then plays only a marginal role, and will thus be omitted in our analysis. For the full expressions of the gauge boson masses and mixings we refer to [27].

JHEP06(2025)254

After the breaking of the LRSM gauge symmetry, the scalar potential leads to mass matrices for all scalar fields depending on the vevs given in eq. (2.3). Their diagonalisation was explicitly solved in [27], which showed that all scalar couplings could be expressed in terms of the scalar physical masses and mixings. The physical states then include, in addition to the SM-like Higgs boson h, several new neutral, singly-charged and doubly-charged scalar eigenstates. As the Δ_L triplet fields are naturally decoupled in the vanishing v_L limit, they will not be further discussed. We then focus on the four remaining neutral scalar fields, and in particular on a potentially light 'Majorana Higgs' field $\Delta \equiv \Delta_R^0$. Among these four neutral scalar fields, the neutral bi-doublet components are required by flavour-changing neutral current constraints to be as heavy as $\sim 20\,\text{TeV}$ [17], and to have tiny mixings to the Δ and h states [32]. Our analysis is consequently restricted to the $(h,\,\Delta)$ subsystem that is characterised by the masses m_h, m_Δ and the mixing angle θ among the h and Δ states. Whereas this mixing is constrained by Higgs invisible decay and exotic searches [67], it can still be as large as approximately 20% in the range of m_Δ values considered in this work. This thus leaves open an interesting window for collider phenomenology.

Neglecting the mixings to the heavier scalar fields,[1] the couplings of the Δ boson to a WW, ZZ and SM $f\bar{f}$ pair are approximately given by

$$C_{\Delta WW} \simeq \sin\theta\, g M_W\,, \qquad C_{\Delta ZZ} \simeq \sin\theta\, \frac{g}{\cos\theta_w} M_Z\,, \qquad C^L_{\Delta f\bar{f}} = C^R_{\Delta f\bar{f}} \simeq \sin\theta\, Y_{f\bar{f}}\,, \tag{2.6}$$

where θ_w stands for the electroweak mixing angle, M_W and M_Z represent the masses of the W and Z boson respectively, and $Y_{f\bar{f}}$ is the Yukawa coupling of a pair of SM fermion-antifermion $f\bar{f}$. The Δ-boson Yukawa couplings are thus proportional to the corresponding SM Higgs couplings via the sine of the mixing angle θ. On the other hand, the triple scalar vertices are much more involved. Again expanding the vertices in the limit of small mixing to the heavier Higgs states and small θ values, they can be written as [32]

$$\begin{aligned} C_{hhh} &\simeq \frac{3g(2-3\theta^2)m_h^2}{4M_W}\,, & C_{hh\Delta} &\simeq \frac{g\theta(\varepsilon\theta-1)(2m_h^2+m_\Delta^2)}{2M_W}\,, \\ C_{h\Delta\Delta} &\simeq \frac{g\theta(\theta+\varepsilon)(m_h^2+2m_\Delta^2)}{2M_W}\,, & C_{\Delta\Delta\Delta} &\simeq \frac{3g\varepsilon(2-3\theta^2)m_\Delta^2}{4M_W}\,, \end{aligned} \tag{2.7}$$

in which $\varepsilon = v/v_R$. In particular, these expressions do not depend on $\tan\beta$, which appears only at higher orders.

Passing on to fermions, the bi-doublet ϕ has Dirac Yukawa coupling to quarks and leptons, while the triplets $\Delta_{L,R}$ have Majorana Yukawa couplings to the left-handed and right-handed leptonic doublets, respectively,

$$\mathcal{L}_Y^{\text{Dirac}} = \bar{Q}_L \left(Y_q\,\phi + \tilde{Y}_q\,\tilde{\phi}\right) Q_R + \bar{L}_L \left(Y_\ell\,\phi + \tilde{Y}_\ell\,\tilde{\phi}\right) L_R + \text{H.c.}\,, \tag{2.8}$$

$$\mathcal{L}_Y^{\text{Maj}} = \bar{L}_L^c i\sigma_2 \Delta_L Y_L L_L + \bar{L}_R^c i\sigma_2 \Delta_R Y_R L_R + \text{H.c.} \tag{2.9}$$

Here, $Y_{q,\ell}$, $\tilde{Y}_{q,\ell}$ are the Dirac Yukawa matrices and $Y_{L,R}$ are the Majorana ones. Spontaneous symmetry breaking induces masses for all the fermions upon insertion of the vevs given

[1] The full expressions are (very) lengthy. While they can be obtained from the FeynRules model developed in [27], they do not offer any evident insights.

JHEP06(2025)254

in eq. (2.3). In the quark sector, the Dirac couplings lead to conventional quark masses and left-handed CKM mixing matrix, together with its right-handed analogue entering the right-handed charged current. As mentioned above, the ($\mathcal{P}$) $\mathcal{C}$ symmetry constrains the Yukawa matrices, with the result that the quark mixing matrices are (almost) identical, up to possible new CP violating phases in the case of a $\mathcal{C}$ symmetry. For our study, we thus safely consider left-handed and right-handed quark mixings to be equal. In the lepton sector, the vevs (2.3) induce standard Dirac masses for the charged leptons, and generate a type I+II seesaw mechanism for the neutrinos. Again, thanks to either a $\mathcal{P}$ or a $\mathcal{C}$ symmetry, the Dirac and Majorana masses are connected [26, 68, 69]. In [27], an explicit solution to the diagonalisation of the lepton sector was found by using the Cayley-Hamilton theorem, while in the case of a $\mathcal{P}$ symmetry an algorithmic approach was developed in [70]. As a result, we adopt the heavy neutrino masses and mixings as physical inputs in addition to the standard light neutrino masses and mixings. These are directly accessible at collider studies through the charged current Lagrangian[2]

$$\mathcal{L}^{\ell}_{cc} \simeq \frac{g_L}{\sqrt{2}} \bar{\ell}_L \gamma_\mu U_\nu \nu \, W^\mu_L + \frac{g_R}{\sqrt{2}} \bar{\ell}_R \gamma_\mu U_N N \, W^\mu_R \,, \tag{2.10}$$

where U_ν effectively coincides with the standard PMNS mixing matrix relevant for the light neutrino eigenstates ν, and U_N represents its analogue for the heavy neutrinos mass eigenstates N. Choosing $m_{N_{1,2,3}}$ and U_N as input parameters, we then consider a benchmark case where the lightest heavy neutrino $N \equiv N_1$ can only decay to electrons and positrons, muons and antimuons, or democratically to all of them.

The Majorana Yukawa coupling of the Δ states to leptons in eq. (2.9) generates not only a mass matrix for the heavy neutrinos $M_N \simeq Y_R v_R$, but also enables the decay modes $\Delta \to N_i N_j$. Thus, the mass eigenstate Δ acts effectively as the Higgs field for the heavy Majorana neutrinos, hence its name 'Majorana Higgs'. The connection is made explicit by writing the ΔNN Feynman rule in terms of the physical input parameters,

$$C^R_{\Delta NN} = \frac{g}{\sqrt{2}} \frac{M_N}{M_{W_R}} \cos\theta \,. \tag{2.11}$$

A similar Feynman rule proportional to $\sin\theta$ couples an NN pair to the SM Higgs boson h, leading not only to the possibility of probing the N mass matrix through the exotic h decay [31], but allowing also for the production of a Δh or a $\Delta\Delta$ pair via gluon fusion [32]. These two mechanisms lie at the heart of this work.

3 Pair and associated production of Δ at pp colliders

The primary production mechanisms for the heavy Higgs boson Δ at proton-proton colliders considered in this work includes its associated production with a SM weak vector boson, $pp \to W^\pm \Delta$ and $pp \to Z\Delta$, as well as with the SM Higgs boson h via gluon fusion, $gg \to h\Delta$. Additionally, we examine the pair production of heavy Higgs states, $gg \to \Delta\Delta$, which also

[2]The charged current includes also a flipped chirality current induced by the Dirac (seesaw) mixing and the $\mathrm{SU}(2)_L$ and $\mathrm{SU}(2)_R$ gauge-boson mixing. The effect is however negligible in the range of N masses considered in the present study.

JHEP06(2025)254

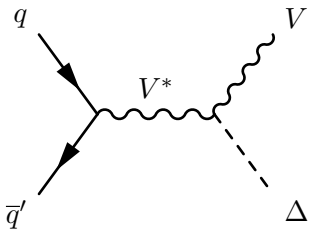


Figure 1. Parton-level Feynman diagram for the 'Δ-strahlung' associated production of a heavy Δ boson with a massive SM weak boson V that can be either a W or a Z boson.

proceeds through gluon fusion. As will be shown in the rest of this work, these channels provide complementary avenues for probing the properties of the heavy Higgs Δ and its connection with heavy neutrinos in the LRSM.

3.1 The Δ-strahlung process, $pp \to V^* \to V\Delta$

Just as for the SM Higgs boson h, the heavy Higgs Δ (of mass m_Δ) can be produced abundantly at proton-proton colliders via the so-called 'Δ-strahlung process', $pp \to V^* \to V\Delta$, where $V = W, Z$ (see the Feynman diagram in figure 1). At leading order, the squared matrix element averaged over initial spins and colours $\overline{|\mathcal{M}_{V\Delta}|}^2$ for the partonic process $q_1\bar{q}_2 \to V\Delta$, is given by

$$\overline{|\mathcal{M}_{V\Delta}|}^2 = C_{\Delta VV}\left(|g_L^{q_1q_2}|^2 + |g_R^{q_1q_2}|^2\right)\frac{M_V^2(2\hat{s}+\hat{t}) - m_\Delta^2(m_V^2-\hat{t}) - \hat{t}(\hat{s}+\hat{t})}{4N_c M_V^2((M_V^2-\hat{s})^2+\Gamma_V^2 M_V^2)}\,, \tag{3.1}$$

where $C_{\Delta VV}$ represents the effective coupling strength of the ΔVV vertex approximately given by eq. (2.6), while $g_{L,R}^{q_1q_2}$ denote the left-handed and right-handed couplings of the weak boson V to the initial quark pair. This expression additionally depends on the standard partonic Mandelstam variables $\hat{s} = (p_1+p_2)^2 = (p_3+p_4)^2$, $\hat{t} = (p_1-p_3)^2 = (p_2-p_4)^2$ and $\hat{u} = (p_1-p_4)^2 = (p_2-p_3)^2$, where $p_{1,2}$ and $p_{3,4}$ denote the four-momenta of the initial-state and final-state partons, respectively. Furthermore, M_V and Γ_V refer to the mass and width of the produced weak boson, and $N_c = 3$ represents the number of colours.

Including the phase-space dependence, the parton-level differential cross section $\mathrm{d}\hat{\sigma}$ is given by

$$\frac{\mathrm{d}\hat{\sigma}(q_1\bar{q}_2 \to V\Delta)}{\mathrm{d}\cos\theta} = \frac{1}{32\pi\hat{s}}\,\lambda\left(1, \frac{m_\Delta^2}{\hat{s}}, \frac{M_V^2}{\hat{s}}\right)\,\overline{|\mathcal{M}_{V\Delta}|}^2\,, \tag{3.2}$$

where $\hat{\lambda}(x,y,z) = x^2+y^2+z^2-2(xy+yz+zx)$ is the usual Källén function. The cosine of the scattering angle, $\cos\theta \in [-1,1]$, can be expressed in terms of the Mandelstam variables as

$$\cos\theta = \frac{\hat{t}-\hat{u}}{\hat{s}\hat{\lambda}\left(1, m_\Delta^2/\hat{s}, M_V^2/\hat{s}\right)}\,. \tag{3.3}$$

The total unpolarised production cross section at proton-proton colliders is then obtained by convoluting the partonic cross section with the universal parton distribution functions (PDFs) f_{q_1} and $f_{\bar{q}_2}$ and summing over all possible initial quark pairs, in accordance with

JHEP06(2025)254

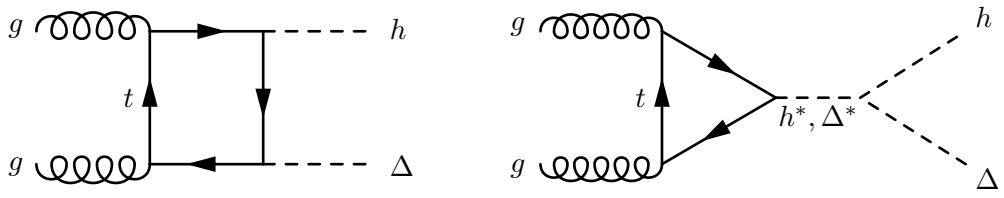


Figure 2. Representative box (left) and triangle (right) Feynman diagrams contributing to the $gg \to h\Delta$ process via top-quark exchanges.

the QCD factorisation theorem. This yields

$$\frac{\mathrm{d}^3\sigma(pp \to V\Delta)}{\mathrm{d}x_1\mathrm{d}x_2\,\mathrm{d}\cos\theta} = \sum_{q_1\bar{q}_2} \left(f_{q_1}(x_1,\mu_F)\, f_{\bar{q}_2}(x_2,\mu_F) + (x_1 \leftrightarrow x_2)\right) \frac{\mathrm{d}\hat{\sigma}(q_1\bar{q}_2 \to V\Delta)}{\mathrm{d}\cos\theta}\,, \tag{3.4}$$

with

$$x_1 \in \left[\frac{(m_\Delta + M_V)^2}{s}, 1\right], \qquad x_2 \in \left[\frac{(m_\Delta + M_V)^2}{s x_1}, 1\right], \tag{3.5}$$

where the hadronic centre-of-mass energy s is related to the partonic one $\hat{s}$ through the Bjorken variables x_1 and x_2 as $\hat{s} = x_1 x_2 s$. In the following, the factorisation scale is set to $\mu_F = \sqrt{\hat{s}}$.

3.2 Heavy Higgs production via gluon fusion

In addition to the Δ-strahlung processes described in section 3.1, the heavy Δ boson can also be produced in pairs or in association with an SM Higgs boson via gluon fusion. In this section, we compute the corresponding loop-induced cross sections at leading order in QCD, accounting for both triangle and box topologies. For the presented analytical results, we consider the limit where the Higgs bosons h and Δ have purely scalar couplings to fermions. This simplification is motivated by the fact that including potential (small) mixings with heavy (pseudo-)scalars A and H states significantly complicates the amplitude without significantly affecting the total cross section. However, our numerical analysis presented later in this paper relies on event generation with MadGraph5_aMC@NLO [71] using the UFO [44, 45] model file developed in [27], where no such assumption is made. Consequently, any small effects of pseudo-scalar mixings on event shapes will be fully incorporated.

The amplitude for $gg \to S_1S_2$ (where $S_1S_2 = h\Delta$ or $\Delta\Delta$) primarily receives contributions from triangle and box diagrams. Representative Feynman diagrams for $gg \to h\Delta$ are shown in figure 2, the diagrams for $gg \to \Delta\Delta$ being similar. The amplitude decomposes as

$$\mathcal{M}(gg \to S_1S_2) = \frac{\alpha_s}{4\pi}\frac{\delta_{ab}}{2}\left(\mathcal{M}^{\mu\nu}_{\triangle} + \mathcal{M}^{\mu\nu}_{\square}\right)\varepsilon_1^{*\mu}(p_1)\varepsilon_2^{*\nu}(p_2)\,, \tag{3.6}$$

where the individual triangle and box contributions can be expressed in terms of a few independent Lorentz structures involving the external four-momenta,

$$\mathcal{M}^{\mu\nu}_{\triangle} = \mathcal{M}^{00}_{\triangle} g^{\mu\nu} + \mathcal{M}^{21}_{\triangle} p_2^\mu p_1^\nu\,, \tag{3.7}$$

$$\mathcal{M}^{\mu\nu}_{\square} = \mathcal{M}^{00}_{\square} g^{\mu\nu} + \mathcal{M}^{21}_{\square} p_2^\mu p_1^\nu + \mathcal{M}^{31}_{\square} p_3^\mu p_1^\nu + \mathcal{M}^{23}_{\square} p_2^\mu p_3^\nu\,. \tag{3.8}$$

JHEP06(2025)254

Here, $\varepsilon_{1,2}$ and $p_{1,2}$ represent the polarisation vectors and four-momenta of the initial-state gluons, while p_3 is the momentum of the S_1 state. There is no dependence on the four-momentum p_4 of the S_2 scalar as we used energy-momentum conservation to remove its dependence. Moreover, the factor $\delta_{ab}/2$ accounts for the trace over the colour indices of the quark running into the loops, and α_s denotes the strong coupling constant. Reducing the tensorial loop integrals to scalar Passarino-Veltman integrals using PACKAGE-X [72, 73], we obtain

$$\mathcal{M}^{00}_{\triangle} = -4 \sum_{S_i,q} Y^q_{S_i}\, C_{S_i S_1 S_2}\, \frac{2B_0 - 8C_{00} + \hat{s}C_0}{\hat{s} - m^2_{S_i} + i\Gamma_{S_i} m_{S_i}}\,, \tag{3.9}$$

$$\mathcal{M}^{21}_{\triangle} = 8 \sum_{S_i,q} Y^q_{S_i}\, C_{S_i S_1 S_2}\, \frac{C_0 - 4C_{12}}{\hat{s} - m^2_{S_i} + i\Gamma_{S_i} m_{S_i}}\,. \tag{3.10}$$

In these expressions, the Passarino-Veltman functions are abbreviated as $B_0 \equiv B_0(\hat{s}, m_q^2, m_q^2)$ and $C_{ij} \equiv C_{ij}(0, \hat{s}, 0, m_q^2, m_q^2, m_q^2)$, following the conventions of LOOPTOOLS [74], with m_q standing for the mass of the quark running in the loop. The UV-divergent pieces in B_0 and C_{00} cancel in $\mathcal{M}^{00}_{\triangle}$, ensuring its (UV-)finiteness. The trilinear scalar couplings $C_{S_i S_j S_k}$ can be approximated as in eq. (2.7) and the quark Yukawa couplings are normalised as in the Lagrangian of eq. (2.8); the m_{S_i} and Γ_{S_i} refer to the mass and width of scalar S_i. Since the box amplitudes are significantly more complex, we provide their analytical expressions in appendix A for completeness.

Squaring the amplitude in eq. (3.6) and averaging over initial-state gluon polarisations yields

$$\begin{aligned}\overline{|\mathcal{M}|^2} = \frac{\alpha_s^2(\mu_R)}{32 N_g^2 \pi^2} \Big\{ & 4|\mathcal{M}^{00}_{\triangle+\square}|^2 + \hat{s}\, \Re\left[\mathcal{M}^{00}_{\triangle+\square} \mathcal{M}^{21*}_{\triangle+\square}\right] \\ & + (m^2_{S_1} - \hat{t})\, \Re\left[\mathcal{M}^{00}_{\triangle+\square} \mathcal{M}^{31*}_{\square}\right] + (m^2_{S_1} - \hat{u})\, \Re\left[\mathcal{M}^{00}_{\triangle+\square} \mathcal{M}^{23*}_{\square}\right] \\ & + \frac{1}{2}(m^2_{S_1} - \hat{t})(m^2_{S_1} - \hat{u})\, \Re\left[\mathcal{M}^{31}_{\square} \mathcal{M}^{23*}_{\square}\right] \Big\},\end{aligned} \tag{3.11}$$

where $\mathcal{M}^{ij}_{\triangle+\square} = \mathcal{M}^{ij}_{\triangle} + \mathcal{M}^{ij}_{\square}$ and $N_g = 8$ represents the number of gluons. The differential partonic cross section follows as

$$\frac{\mathrm{d}\hat{\sigma}}{\mathrm{d}\cos\theta} = \frac{1}{1 + \delta_{S_1 S_2}} \frac{1}{32\pi\hat{s}}\, \hat{\lambda}\left(1, \frac{m^2_{S_1}}{\hat{s}}, \frac{m^2_{S_2}}{\hat{s}}\right) \overline{|\mathcal{M}|^2}\,, \tag{3.12}$$

where the scattering angle $\cos\theta$ is given by

$$\cos\theta = \frac{\hat{t} - \hat{u}}{\hat{s}\, \hat{\lambda}\left(1, m^2_{S_1}/\hat{s}, m^2_{S_2}/\hat{s}\right)}\,. \tag{3.13}$$

The total hadronic cross section is finally obtained by convoluting the partonic cross section with the gluon PDFs,

$$\frac{\mathrm{d}^3\sigma}{\mathrm{d}x_1 \mathrm{d}x_2\, \mathrm{d}\cos\theta} = f_g(x_1, \mu_F) f_g(x_2, \mu_F)\, \frac{\mathrm{d}\hat{\sigma}}{\mathrm{d}\cos\theta}\,, \tag{3.14}$$

JHEP06(2025)254

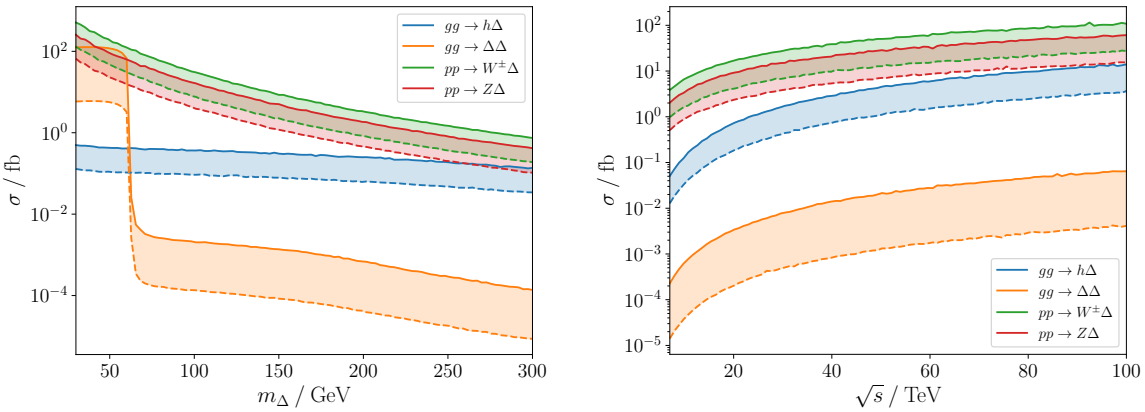


Figure 3. Production cross sections for the different Δ production processes studied in this work. In the left panel, we present cross sections as a function of m_Δ at $\sqrt{s} = 14$ TeV while in the right panel, we show cross sections as a function of $\sqrt{s}$ for a fixed $m_\Delta = 142$ GeV. In both panels, solid and dashed lines correspond to $\sin\theta = 0.1$ and 0.05, respectively.

with

$$x_1 \in \left[\frac{(m_{S_1} + m_{S_2})^2}{s}, 1\right], \qquad x_2 \in \left[\frac{(m_{S_1} + m_{S_2})^2}{s\, x_1}, 1\right]. \tag{3.15}$$

The phase-space integration is detailed in appendix B and can be non-trivial because of resonant effects, especially for $gg \to \Delta\Delta$ production. As in the SM process $gg \to hh$, the dominant contribution to the $gg \to h\Delta$ cross section arises from box diagrams, which interfere destructively with the triangle contributions.

3.3 Cross sections for Δ production at proton-proton colliders

In figure 3, we present the production cross sections for the different Δ production modes introduced in sections 3.1 and 3.2. The left panel shows the variation of the cross sections with the heavy Higgs mass m_Δ for proton-proton collisions at $\sqrt{s} = 14$ TeV, using the NLO set of NNPDF40 parton densities [75] (i.e., `NNPDF40_nlo_as_01180`, that corresponds to the identifier 331700 in LHAPDF 6.5.4 [76]). In this figure, we explore two benchmark values for the scalar mixing angle, $\sin\theta = 0.1$ (solid lines) and $\sin\theta = 0.05$ (dashed lines). In the right panel, we instead examine the dependence of the rate on $\sqrt{s}$, fixing $m_\Delta = 142$ GeV and varying $\sin\theta$ as above, between 0.05 and 0.1.

Our results have been derived analytically and cross-validated against MG5aMC, with the Passarino-Veltman functions being evaluated using a custom Python interface to LoopTools [74]. They indicate that associated production $pp \to V\Delta$ maintains sizeable cross sections above 1 fb across the entire considered parameter range. For $m_\Delta < m_h/2$, resonant pair production via gluon fusion, $gg \to h \to \Delta\Delta$, reaches comparable rates before sharply decreasing beyond the threshold. On the other hand, the associated Higgs production mode, $gg \to h\Delta$, is somewhat subdominant but remains significant enough to lead to a substantial event yield at the high-luminosity phase of the LHC.

JHEP06(2025)254

4 Heavy Higgs and neutrino decays and branching ratios

In this section, we derive analytical expressions for all relevant decay modes of the heavy Higgs boson Δ and the heavy right-handed neutrino N. Additionally, we present numerical results to identify viable regions of parameter space where the decay $\Delta \to NN$ is either dominant or sufficiently sizeable for heavy Higgs production to yield a significant number of signal events at colliders. The study made in this section therefore provides insights into the interplay between the different decay channels of the considered states, and helps to delineate the region of the parameter space where left-right models could be probed to a new signatures.

4.1 Δ decays

Depending on its mass m_Δ and the mixing parameters of the scalar sector, the heavy Higgs boson Δ can undergo various two-body and three-body decays into different final states. We begin our analysis by introducing the relevant analytical expressions, before examining their numerical behaviour for specific choices of input parameters. The partial decay widths related to two-body decay channels of Δ are given by

$$\Gamma(\Delta \to hh) = \frac{|C_{\Delta hh}|^2}{32\pi m_\Delta}\sqrt{1-\frac{4m_h^2}{m_\Delta^2}}\,, \tag{4.1}$$

$$\Gamma(\Delta \to VV) = \frac{|C_{\Delta VV}|^2}{16\pi m_\Delta(1+\delta_V)}\left(2+\frac{m_\Delta^2}{4M_V^2}\right)\sqrt{1-\frac{4M_V^2}{m_\Delta^2}} \quad \text{with } V = W,\, Z\,, \tag{4.2}$$

$$\Gamma(\Delta \to f\bar{f}) = \frac{m_\Delta}{16\pi}\sqrt{1-\frac{4m_f^2}{m_\Delta^2}}\left[\left(1-\frac{2m_f^2}{m_\Delta^2}\right)\left(|C_L|^2+|C_R|^2\right) - 4\frac{m_f^2}{m_\Delta^2}\Re(C_L C_R^*)\right], \tag{4.3}$$

where the symmetry factors are $\delta_Z = 1$ and $\delta_W = 0$. The coefficients $C_{\Delta hh}$ and $C_{\Delta VV}$ represent the trilinear scalar coupling and the scalar-vector interaction strengths, respectively, while the $C_{L,R}$ couplings encode the Yukawa interactions of the Δ state with fermions. In particular, for SM fermions, we have $C_L \approx C_R$ in the limit of negligible mixing between the scalar state Δ and the pseudo-scalar state A. On the contrary, in the case of $\Delta \to NN$, the right-handed coupling C_R is dominant, with an expression given by eq. (2.11). If m_Δ lies below one or more of the two-body kinematic thresholds, the Δ decays via three-body processes mediated by off-shell weak bosons V or Higgs boson h, that can contribute significantly. For an off-shell SM Higgs exchange, the differential decay width is given by

$$\frac{\mathrm{d}\Gamma(\Delta \xrightarrow{h^*} hf\bar{f})}{\mathrm{d}\hat{s}_1} = \frac{N_c\sqrt{\hat{\lambda}(1,\hat{s}_1,\hat{m}_h^2)\hat{\lambda}(1,\hat{m}_f^2,\hat{m}_f^2)}|C_{\Delta hh}|^2 m_\Delta^3}{256\pi^3((\hat{s}_1 m_\Delta^2 - m_h^2)^2 + (m_h\Gamma_h)^2)}\hat{s}_1\left(1-4\frac{\hat{m}_f^2}{\hat{s}_1}\right)|Y_{ff}|^2\,, \tag{4.4}$$

where Y_{ff} denotes the Yukawa coupling of the SM Higgs to a fermion f of mass m_f. The 'hatted' variables appearing in this expression are defined as $\hat{s}_1 = s_1/m_\Delta^2$ and $\hat{m}_i = m_i/m_\Delta$, while m_h and Γ_h refer to the SM Higgs boson mass and width. The total decay width is then obtained by integrating the differential partial width over $\hat{s}_1$ over the range

$$4\hat{m}_f^2 \le \hat{s}_1 \le (1-\hat{m}_h)^2\,. \tag{4.5}$$

JHEP06(2025)254

For three-body decays via an off-shell vector boson, the expression of the corresponding partial decay width reads

$$\begin{aligned}\frac{\mathrm{d}\Gamma(\Delta \xrightarrow{V^*} V f_i \bar{f}_j)}{\mathrm{d}\hat{s}_1} &= \frac{N_c\sqrt{\lambda_V \lambda_{ij}}|C_{\Delta VV}|^2 m_\Delta^3}{256\pi^3((\hat{s}_1 m_\Delta^2 - M_V^2)^2 + (m_V\Gamma_V)^2)}\left(\hat{s}_1 + \frac{\lambda_V}{12\hat{M}_V^2}\right) \\ &\times \left[\left(2 - \Sigma_{ij}\left(1 + \frac{3\beta_V^2\lambda_V}{12\hat{M}_V^2\hat{s}_1 + \lambda_V}\right) - \Delta_{ij}^2\left(1 - \frac{3\beta_V^2\lambda_V}{12\hat{M}_V^2\hat{s}_1 + \lambda_V}\right)\right)\right. \\ &\times \left.\left(|g_L|^2 + |g_R|^2\right) + 12\frac{\hat{m}_i\hat{m}_j}{\hat{s}_1}\left(1 - \frac{\beta_V^2\lambda_V}{12\hat{M}_V^2\hat{s}_1 + \lambda_V}\right)\Re(g_L g_R^*)\right],\end{aligned} \tag{4.6}$$

where we defined

$$\begin{aligned}\beta_V = 1 - \frac{\hat{s}_1}{\hat{M}_V^2}, \qquad \lambda_V = \hat{\lambda}(1, \hat{s}_1, \hat{M}_V^2), \qquad \lambda_{ij} = \hat{\lambda}(1, \hat{m}_i^2, \hat{m}_j^2) \\ \Sigma_{ij} = \hat{m}_i^2 + \hat{m}_j^2, \qquad \Delta_{ij} = \hat{m}_i^2 - \hat{m}_j^2.\end{aligned} \tag{4.7}$$

Here, $g_{L,R}$ denote the left- and right-handed gauge couplings of the involved vector boson to fermions. The full partial decay width is then obtained after integration over $\hat{s}_1$ within the boundaries

$$(\hat{m}_i + \hat{m}_j)^2 \leq \hat{s}_1 \leq (1 - \hat{M}_V)^2. \tag{4.8}$$

Finally, we note that the loop-induced Δ decays to $\gamma\gamma$, γZ, and gg final states are also possible. However, these channels are subdominant [32] and will not be considered further.

In figure 4, we present the dominant branching ratios of the heavy Higgs Δ as a function of its mass m_Δ. The left panel illustrates the impact of varying the sine of the mixing angle, $\sin\theta$, between 5% (solid lines) and 10% (dashed lines), while keeping the mass of the right-handed W boson fixed at $M_{W_R} = 6\,\mathrm{TeV}$. The thickness of the band embeds variations of $\sin\theta$ between these two values. In contrast, the right panel explores the dependence on M_{W_R} after setting $\sin\theta = 10\%$ and varying M_{W_R} between 6 TeV (solid) and 20 TeV (dashed), the variation being again embedded in the band thickness. In both cases, we assume a fixed heavy neutrino mass of $m_{N_i} = 45\,\mathrm{GeV}$. To investigate the impact of the heavy neutrino mass, we display in figure 5 the same branching ratios, but now setting $m_{N_i} = m_\Delta/3$.

As can be observed, the branching ratio of the decay $\Delta \to NN$ (red curve) dominates over a broad range of m_Δ values. However, it exhibits a slight decrease with increasing $\sin\theta$, which is attributable to a relative enhancement of the competing two-body decay $\Delta \to b\bar{b}$ as well as the three-body decays $\Delta \to Xf\bar{f}$ (where $X = W, Z, h$). The branching ratio $\mathrm{BR}(\Delta \to NN)$ further decreases for increasing M_{W_R} values, a consequence of eq. (2.11). Since the heavy neutrino Yukawa couplings scale as $y_N \sim m_N/M_{W_R}$, a larger W_R-boson mass leads to a smaller Yukawa coupling and thus a suppressed partial decay width for $\Delta \to NN$, assuming a fixed m_N. This interplay between M_{W_R} and $\mathrm{BR}(\Delta \to NN)$ has important phenomenological implications when considering the production of heavy neutrinos via Δ decays at colliders. As previously discussed in section 3, the production cross section of Δ increases with $\sin\theta$. This means that although $\mathrm{BR}(\Delta \to NN)$ decreases with $\sin\theta$, the overall number of heavy neutrino events produced via intermediate Δ production can remain significant due to the

JHEP06(2025)254

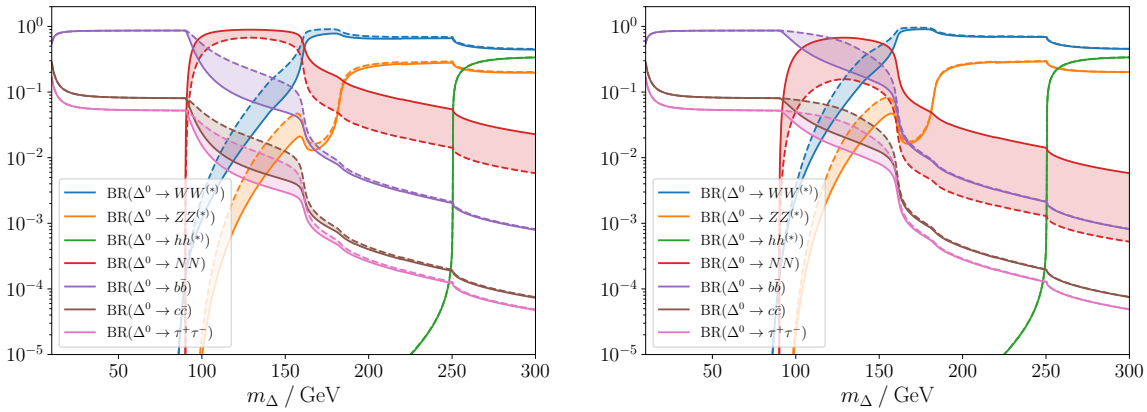


Figure 4. Branching ratios of Δ for $m_{N_i} = 45\,\text{GeV}$. In the left panel, we consider a setup where we have fixed M_{W_R} to 6 TeV, with the solid and dashed lines showing predictions for $\sin\theta = 0.05$ and 0.1 respectively. In the right panel, we fix $\sin\theta = 0.1$ and vary M_{W_R} from 6 TeV (solid) to 20 TeV (dashed).

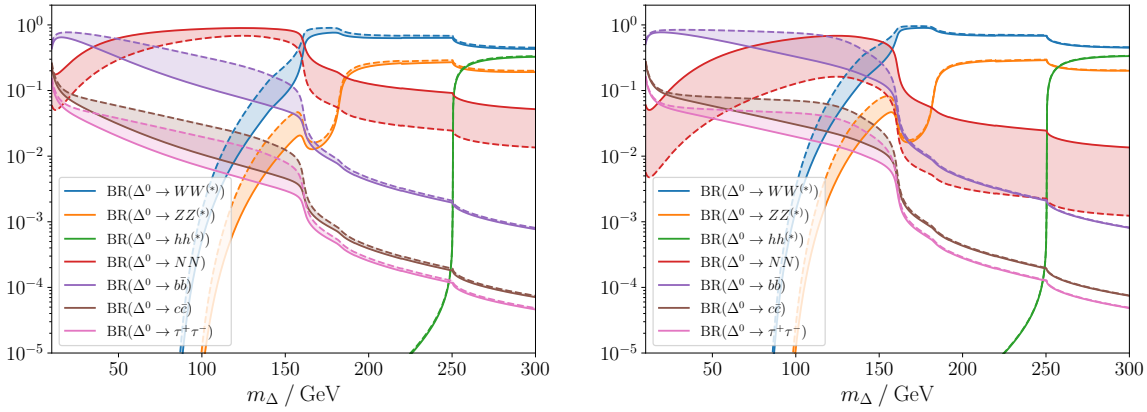


Figure 5. Same as figure 4 for $m_{N_i} = m_\Delta/3$.

enhanced production rate. This effect is illustrated in figure 6, where we display the product of the production cross section $\sigma(pp \to \Delta)$ (distinguishing the different production channels) with the branching ratio $\text{BR}(\Delta \to NN)$ for different values of m_Δ and M_{W_R} (see caption for details). Notably, for $\sin\theta \gtrsim 1\%$, the variation in $\sigma \times \text{BR}$ is relatively mild, justifying our choice of $\sin\theta = 10\%$ for the remainder of our analysis.

4.2 Right-handed neutrino decay and lifetime

In the minimal LRSM, the heavy right-handed neutrinos N typically decay via off-shell W- and W_R-boson exchanges, leading to three-body final states. However, if their masses are sufficiently large, two-body decays into a charged lepton and an on-shell SM-like W boson can become relevant. The decay width for a massive fermion transitioning into another fermion and a massive vector boson is given by

$$\Gamma(f_1 \to f_2 V) = \frac{m_1 \lambda_{f_2 V}}{16\pi}\left[\frac{|g_L|^2 + |g_R|^2}{2}\left(3\left(1 + \frac{m_2^2 - M_V^2}{m_1^2}\right) + \lambda_{f_2 V}\frac{m_1^2}{M_V^2}\right) - \frac{m_2}{m_1}\Re(g_L g_R^*)\right], \tag{4.9}$$

JHEP06(2025)254

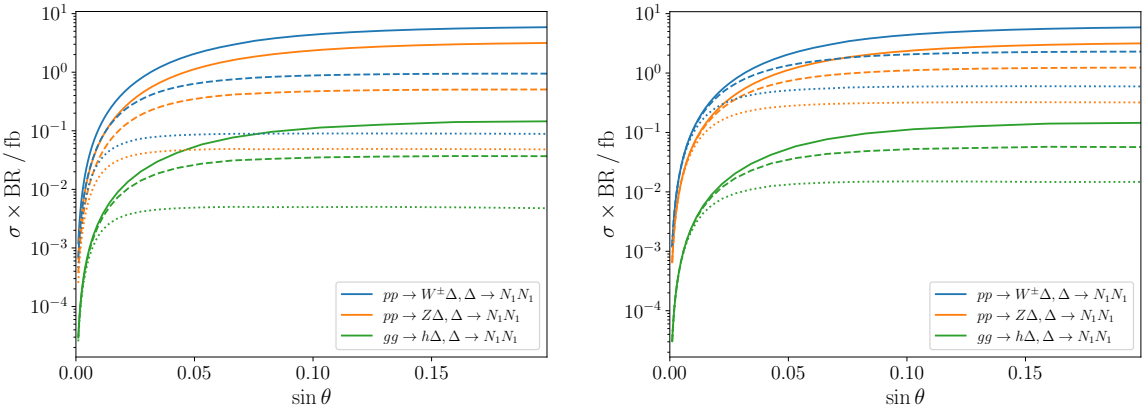


Figure 6. Product of the dominant cross sections for Δ production with the branching ratio $\mathrm{BR}(\Delta \to N_1N_1)$, shown as a function the sine of the scalar mixing angle θ. We consider $W\Delta$ production (blue), $Z\Delta$ production (orange) and $h\Delta$ production (green), and different mass spectra. In the left panel, we vary m_Δ and fix it to 135 GeV (solid), 160 GeV (dashed) and 180 GeV (dotted), with $m_{N_1} = m_\Delta/3$. In the right panel, we instead vary M_{W_R} and fix it to 6 TeV (solid), 10 TeV (dashed) and 20 TeV (dotted) with $m_\Delta = 135$ GeV and $m_{N_1} = 45$ GeV.

where $\lambda_{f_2V} = \hat{\lambda}(1, m_2^2/m_1^2, M_V^2/m_1^2)$, with m_1 and m_2 denoting the masses of the fermions f_1 and f_2, respectively, and $g_{L,R}$ representing the gauge couplings associated with the boson V.

For the full three-body decay width of a heavy neutrino into a charged lepton and a quark-antiquark pair, both W_L and W_R interactions contribute. The relevant couplings arise either via left-right mixing, which links the SM fields to the heavy neutrino, or through direct Dirac neutrino mixing. In the parameter space of interest where $m_N \lesssim m_W$, the dominant contribution to the three-body decay $N \to \ell^{\pm} q\bar{q}'$ comes from W_R-boson exchange. The corresponding partial decay width can be approximated as [61]

$$\Gamma(N_k \to \ell_\alpha^{\pm} q_i \bar{q}_j) \simeq 2\frac{\alpha_w^2 m_{N_k}^5}{128\pi M_{W_R}^4} \left|V_{R,ij}^{\mathrm{CKM}}\right|^2 \left|U_{R,\alpha k}^{\mathrm{PMNS}}\right|^2 (1 - 8x + 8x^2 - x^4 - 12x^2 \log x)\,, \quad (4.10)$$

where $x = m_q^2/m_{N_k}^2$ with m_q being the heavier of the two final-state quarks. Moreover, the matrices V_R^{CKM} and U_R^{PMNS} represent the right-handed CKM and PMNS matrices, respectively, and α_w is the weak coupling constant. The full expression for the partial width $\Gamma(N_k \to \ell_\alpha^{\pm} q_i \bar{q}_j)$, including interference effects between W_L and W_R contributions, as well as the impact of the masses of the charged lepton and quarks, is too lengthy to be displayed here. However, in our numerical analysis, we fully account for these effects, which have been shown to be small for $m_N \gtrsim 10$ GeV [61]. Furthermore, we neglect hadronisation effects, which become significant for $m_N \lesssim 10$ GeV. Consequently, our collider analysis is limited to scenarios with heavier neutrinos.

Although heavy neutrinos can decay through multiple channels, their total decay width can be quite small. As a result, their collider signatures may include displaced vertices and leptons. To compute the number of events where a heavy neutrino decays at a given transverse displacement d_{xy} (which corresponds to the location of the secondary vertex, rather than the transverse impact parameter), we must convolute the production cross sections

JHEP06(2025)254

$\sigma(pp \to h\Delta, V\Delta)$ with the exponential probability distribution governing particle decays,

$$P_N(d_{xy}) = \frac{1}{\langle d_{xy}\rangle} \exp\left(-\frac{d_{xy}}{\langle d_{xy}\rangle}\right) . \tag{4.11}$$

Here, the average transverse displacement is given by

$$\langle d_{xy}\rangle = \frac{p_T^{\rm lab}(N)}{m_N}\tau_N \,, \tag{4.12}$$

where τ_N is the proper lifetime of the decaying heavy neutrino. Since this depends on the transverse momentum of the heavy neutrino in the laboratory frame $p_T^{\rm lab}(N)$, the average transverse displacement must be computed on an event-by-event basis. To determine $p_T^{\rm lab}(N)$, we must boost the heavy neutrino's four-momentum from the rest frame of the produced Δ state into the laboratory frame. This transformation is performed using the boost vector $\vec{\beta}_\Delta$ and corresponding Lorentz factor γ_Δ,

$$\vec{p}_N^{\,\rm lab} = \vec{p}_N^{\,\Delta} + \gamma_\Delta \vec{\beta}_\Delta \left(\frac{\gamma_\Delta}{1+\gamma_\Delta}\vec{\beta}_\Delta \cdot \vec{p}_N^{\,\Delta} - E_N^\Delta\right) , \tag{4.13}$$

where, in this expression, the superscript Δ denotes the rest frame of Δ. Consequently, the quantities E_N^Δ and $\vec{p}_N^{\,\Delta}$ represent the heavy neutrino energy and momentum in the Δ rest frame. Moreover, the Δ boost and Lorentz factor are obtained from its energy and momentum in the laboratory frame $E_\Delta^{\rm lab}$ and $\vec{p}_\Delta^{\,\rm lab}$, as $\vec{\beta}_\Delta = \vec{p}_\Delta^{\,\rm lab}/E_\Delta^{\rm lab}$, $\gamma_\Delta = (1-|\vec{\beta}_\Delta|^2)^{-1/2}$. In order to determine the fully differential cross section for heavy neutrino N production and decay via intermediate Δ production, we need to calculate the cross sections for the three-body processes $pp \to hNN$ and $pp \to VNN$. To achieve this, we begin by partitioning the three-body phase space $\Phi_3(\hat{s})$ into two components: a two-body phase-space component $\Phi_2(\hat{s}; m_{h,V}^2, \hat{s}_\Delta)$ relevant for the $2 \to 2$ production process ($pp \to h\Delta$ or $pp \to V\Delta$), and another two-body phase-space component $\Phi_2(\hat{s}_\Delta; m_N^2, m_N^2)$ which corresponds to the $1 \to 2$ decay process $\Delta \to NN$. The full phase space is then factorised as

$$\Phi_3(\hat{s}) = \int \mathrm{d}\hat{s}_\Delta \, \Phi_2(\hat{s}; m_{V,h}^2, \hat{s}_\Delta)\, \Phi_2(\hat{s}_\Delta; m_N^2, m_N^2) \,. \tag{4.14}$$

To simplify this expression further, we rely on the narrow-width approximation that can be enforced on the intermediate Δ propagator,

$$\frac{1}{(\hat{s}_\Delta - m_\Delta^2)^2 + (\Gamma_\Delta m_\Delta)^2} \simeq \frac{\pi}{\Gamma_\Delta m_\Delta}\delta(\hat{s}_\Delta - m_\Delta^2) \,, \tag{4.15}$$

which leads to a factorised form for the fully differential cross section,

$$\frac{\mathrm{d}\sigma(pp \to hNN)}{\mathrm{d}x_1\mathrm{d}x_2\mathrm{d}\cos\theta_\Delta\mathrm{d}\phi_N\,\mathrm{d}\cos\theta_N} \simeq \frac{\mathrm{d}\sigma(pp \to h\Delta)}{\mathrm{d}x_1\mathrm{d}x_2\,\mathrm{d}\cos\theta_\Delta}\,\frac{1}{\Gamma_\Delta}\,\frac{\mathrm{d}\Gamma(\Delta \to NN)}{\mathrm{d}\phi_N\,\mathrm{d}\cos\theta_N} \,. \tag{4.16}$$

In this expression, ϕ_N and θ_N are the azimuthal and polar angles of the heavy neutrino N in the rest frame of the Δ scalar boson, while θ_Δ is the polar angle of the Δ state in the laboratory frame. Additionally, the dependence on the azimuthal angle ϕ_Δ has been trivially omitted due to the rotational symmetry along the collision axis. For illustration,

JHEP06(2025)254

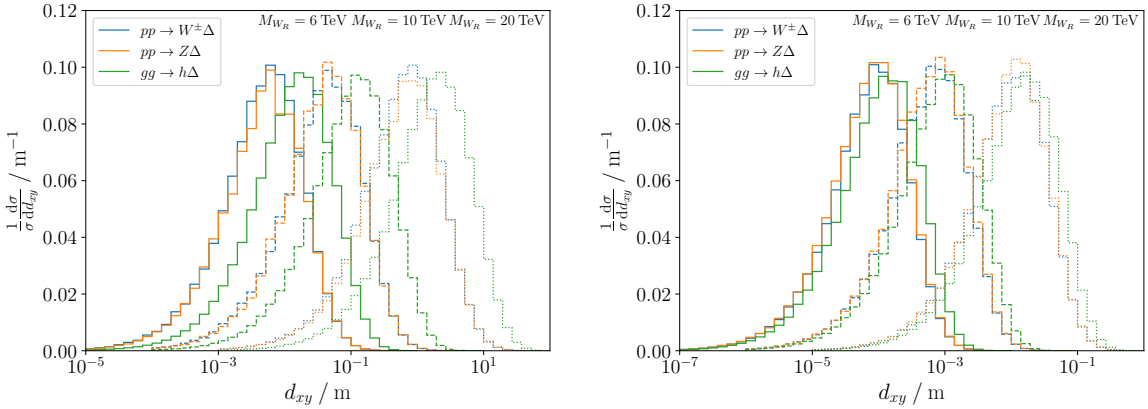


Figure 7. Normalised distributions of the transverse displacement of heavy neutrinos originating from the decay of a Δ scalar produced in association with a W boson (blue), Z boson (orange), or Higgs boson h (green). We consider scenarios where $m_\Delta = 60$ GeV and $m_{N_1} = 20$ GeV (left), as well as $m_\Delta = 135$ GeV and $m_{N_1} = 45$ GeV (right). Solid, dashed and dotted lines indicate $M_{W_R} = 6\,, 10\,, 20$ TeV respectively.

this expression and the following ones considers a process featuring a final-state SM Higgs boson h. Similar expressions can be naturally derived for the other two production processes.

In order to determine the event yields as a function of the heavy neutrino displacement, we note that the differential partial decay width $\mathrm{d}\Gamma(\Delta \to NN)$ is independent of ϕ_N and θ_N, so the angular integration of the expression in eq. (4.16) can be trivially performed. However, to estimate the transverse displacement of the heavy neutrino N in the laboratory frame, we must calculate its transverse momentum $p_T^{\mathrm{lab}}(N)$, which retains a dependence on ϕ_N, θ_N and θ_Δ. The differential event distribution $\mathrm{d}\mathcal{N}$ with respect to the transverse displacement d_{xy} can then be determined and written as

$$\frac{\mathrm{d}\mathcal{N}}{\mathrm{d}(d_{xy})} = \mathcal{L} \int \frac{\mathrm{d}\sigma(pp \to h\Delta)}{\mathrm{d}x_1 \mathrm{d}x_2\, \mathrm{dcos}\,\theta_\Delta} \frac{\mathrm{BR}(\Delta \to NN)}{4\pi} \frac{\mathrm{e}^{-d_{xy}/\langle d_{xy}\rangle}}{\langle d_{xy}\rangle} \mathrm{d}x_1\, \mathrm{d}x_2\, \mathrm{dcos}\,\theta_\Delta\, \mathrm{d}\phi_N\, \mathrm{dcos}\,\theta_N\,, \tag{4.17}$$

where $\mathcal{L}$ represents the integrated luminosity. To estimate the number of events $\mathcal{N}$ decaying with a certain transverse displacement $[d_{xy}^{\min}, d_{xy}^{\max}]$, it is finally sufficient to integrate this result over the displacement range. This gives, up to detector efficiencies,

$$\mathcal{N} = \int_{d_{xy}^{\min}}^{d_{xy}^{\max}} \frac{\mathrm{d}\mathcal{N}}{\mathrm{d}(d_{xy})} = \int \mathrm{d}\Phi_3 \frac{\mathrm{d}\sigma}{\mathrm{d}\Phi_3} \left(e^{-\frac{d_{xy}^{\min}}{\langle d_{xy}\rangle}} - e^{-\frac{d_{xy}^{\max}}{\langle d_{xy}\rangle}} \right). \tag{4.18}$$

This expression can be refined further to account for the displaced vertex related to the decay of the second produced heavy neutrino, which leads to an additional exponential distribution. Since $\vec{p}_{N_1}^{\,\Delta} = -\vec{p}_{N_2}^{\,\Delta}$ (where the notation N_1 and N_2 stand for the two final-state neutrinos), the transverse momentum $p_T^{\mathrm{lab}}(N_2)$ can be immediately derived, leading to an equivalent expression for $\langle d_{xy}(N_2)\rangle$.

In figure 7, we show the (semi-)analytically obtained distributions of events with respect to their transverse displacement d_{xy} for various example mass spectra. The presented results rely on the analytical expressions derived in section 3 and this section, and have been further

JHEP06(2025)254

validated against Monte Carlo simulations. For this purpose, hard-scattering events were generated using MG5aMC, with heavy particle decays handled by MadSpin [77] and MadWidth [78], while parton showering and hadronisation were simulated with Pythia 8 [79]. Event analysis was performed using the MadAnalysis 5 framework [80–83].

The colour code in figure 7 represents displaced N decays from $pp \to W^{\pm}\Delta$ (blue), $pp \to Z\Delta$ (orange), and $gg \to h\Delta$ (green) production. In the left panel, we fix $m_{\Delta} = 60\,\text{GeV}$ and $m_{N_1} = 20\,\text{GeV}$, while in the right panel, we choose instead $m_{\Delta} = 135\,\text{GeV}$ and $m_{N_1} = 45\,\text{GeV}$. Finally, solid, dashed, and dotted lines correspond to $M_{W_R} = [6, 10, 20]\,\text{TeV}$. The displacement relevant for heavy neutrinos originating from $gg \to h\Delta$ production is slightly larger compared to that stemming from Δ-strahlung processes ($pp \to V\Delta$), due to the higher production threshold and therefore larger boost of the Δ state. Additionally, the displacement distribution is shifted to larger values with growing M_{W_R} masses. Consequently, for very heavy W_R bosons, a significant displacement ($d_{xy} > 0.1\,\text{mm}$) can be expected for many events. For light neutrinos N and very heavy W_R boson, the expected displacement can even exceed the typical size of the inner tracker of an LHC detector ($R_{\text{Tracker}} \lesssim 30\,\text{cm}$), and the decay could occur in the muon system ($8\,\text{m} \lesssim R_{\text{MS}} \lesssim 13\,\text{m}$).

5 Sensitivities at run-3 and HL-LHC

Up to the present day, a plethora of experimental searches for a heavy W_R boson (often called a W' boson) have been performed across a variety of channels. Among these, di-jet or $t\bar{b}$ resonance searches probe the resonant production and decay of the W_R boson into two light jets [46, 47] or a $t\bar{b}$ pair [48, 49], and place a lower bound on the mass of the W_R boson of $M_{W_R} \gtrsim 4.5\,\text{TeV}$. Furthermore, searches for a single high-p_T lepton accompanied by large missing transverse energy have been conducted by both the ATLAS and CMS collaborations [57–59]. These provide competitive constraints on the $pp \to W_R \to \ell N$ channel, particularly if the heavy neutrino N is long-lived enough to escape detection.

However, one of the most promising LRSM signals stems from the so-called Keung-Senjanović (KS) mechanism [52], where the process $pp \to \ell^+ N$ is followed by the heavy neutrino decay $N \to \ell^+ jj$. This signature hence features a high-p_T lepton alongside a same-sign secondary lepton and a pair of light jets originating from N decay. In addition, a variant of the KS mechanism has also been recently proposed in the context of third-generation quarks, thereby relying on the process $pp \to N \to \ell^+ N$ followed by the decay $N \to \ell^+ t\bar{b}$ [53]. Searches for the KS process have been conducted by both the ATLAS and CMS collaborations [84, 85]. They also account for possible displacements due to a displaced heavy neutrino decay, and consider scenarios where several final-state particles merge into a single detector-level object due to the large boost of the heavy neutrino N. Depending on the heavy neutrino mass, these searches typically constrain $M_{W_R} \gtrsim 6 - 7\,\text{TeV}$ for $m_N \gtrsim 50\,\text{GeV}$.

In contrast, the scalar sector of the LRSM has received significantly less experimental attention. In the following subsections, we propose searches for Δ production and decay, and assess numerically their potential via a dedicated and extensive sensitivity analysis.

5.1 Displaced Majorana Higgses

The dominant production channels for the Δ Higgs boson across most of the parameter space involve the so-called Δ-strahlung processes, where it is produced in association with an SM

JHEP06(2025)254

vector boson, i.e. $pp \to V\Delta$ with $V = W^{\pm}, Z$ (see figure 3). The subsequent decay of the Δ boson via the $\Delta \to NN$ channel and the heavy neutrino decay $N \to \ell^{\pm} jj$ result in a final state comprising multiple leptons and jets. Moreover, these decays often exhibit sizeable displacements, as described in section 4.2, thus occurring within the inner tracker or even in the muon system of a typical LHC detector. We recall that this is particularly true if the W_R boson is significantly heavy and the heavy neutrino N remains relatively light, *ie.* the mass configuration to which our study is dedicated.

To analyse this signal, we perform detailed simulations using the FeynRules/UFO model developed in [27]. Hard-scattering event generation, including the decays of unstable heavy particles, is carried out using MG5aMC, MadSpin, and MadWidth. The generated events are then processed with Pythia 8 for parton showering and hadronisation, followed by a fast detector simulation using Delphes [86] that relies on the anti-k_T algorithm [87] as implemented in FastJet [88] for event reconstruction. Event generation is achieved by assuming the following input model parameters,

$$\tan\beta = 0.1\,, \qquad \sin\theta = 0.1\,, \qquad \eta = \phi = 0\,, \qquad m_{N_1} = m_{\Delta}/3\,, \tag{5.1}$$

and we assume that all other LRSM heavy states to be sufficiently decoupled so that their contributions can be safely neglected. Additionally, we set the right-handed analogue of the PMNS matrix to be diagonal, and we focus on final states only containing electrons and muons.

We preselect events containing at least two isolated lepton tracks, each satisfying the transverse momentum requirement $p_T(\ell) > 10$ GeV and the pseudo-rapidity constraint $|\eta(\ell)| < 2.4$. Furthermore, each lepton must be separated, in the transverse plane, from the nearest jet j_c by $\Delta R(\ell, j_c) > 0.4$. To improve the reconstruction of soft leptons which are characteristic of the mass scales probed, we modify several Delphes parameters. Specifically, we adopt the standard ATLAS detector card while setting $\Delta R_{\rm max} = 0.3$ (corresponding to the lepton cone size) and $(p_T)^{\rm max}_{\rm ratio} = 0.12$ for lepton isolation, following the loose lepton criteria outlined in [89]. We validate these modifications by comparing with a soft-lepton implementation within the SFS framework [83, 90, 91] as integrated in MadAnalysis 5. The analysis is then divided into two distinct signal regions, each targeting specific decay displacements. We first consider a 'Tracker Region' where we require the presence of two displaced vertices each associated with a lepton track, with their transverse displacement satisfying 0.1 mm $< d_{xy}(\ell_1, \ell_2) <$ 30 cm. This ensures that heavy neutrino decays occur within the inner tracker volume of a typical LHC detector (see for instance [92]). Secondly, we define a 'Muon System Region' corresponding to the selection of events where the heavy neutrino decays occur within the muon system, imposing a transverse displacement criterion of 8 m $< d_{xy} <$ 13 m.

The goal of this analysis is to pioneer an exploration of the LHC sensitivity to the signal proposed. Therefore, we only consider the simple cuts described above. We nevertheless emphasise that any more precise estimate would require a full detector simulation including in particular a more accurate description of muon system clustering, a task that lies well beyond our scope.

To control backgrounds, we consider hadronic decays of the hard-scattering W or Z bosons, and require two same-sign leptons. We therefore simulate SM backgrounds from

JHEP06(2025)254

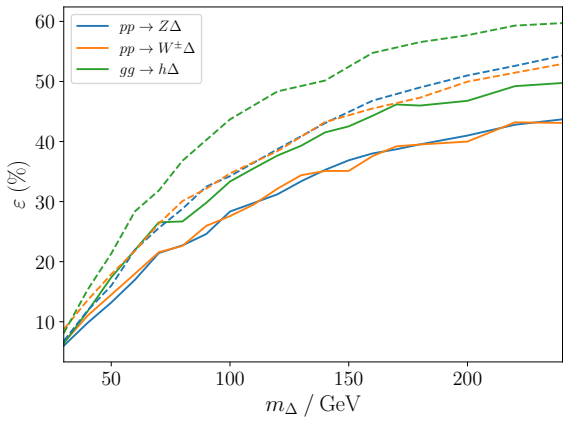


Figure 8. Signal efficiencies for Δ production (and decay into displaced leptons and jets) in association with a W boson (blue), Z boson (orange), or Higgs boson h (green). Solid and dashed lines correspond to di-electron and di-muon final states, respectively.

$t\bar{t} + X$ production with $X = h, Z, W$, as well as for the multiboson processes $pp \to VV$ and $pp \to VVV$ with $V = W^{\pm}, Z$. After applying the selection criteria, we impose an additional requirement on the invariant mass of the reconstructed vertices, $m_{\text{vert}} > 10$ GeV, which eliminates practically all backgrounds. The remaining background events then primarily originate from cosmic rays, which can be effectively vetoed following methods such as those described in [93]. As a result, we consider our analysis to be essentially background-free and define the signal significance as

$$Z = \sqrt{S}\,. \tag{5.2}$$

The signal hypothesis is then rejected at 95% confidence level if the number of signal events $S \gtrsim 3$.

The signal selection outlined above leads to efficiencies of approximately 40–50% across most of the parameter space and for all Δ production channels. Tables 1–2 in appendix C present signal efficiencies obtained with MadAnalysis and our SFS implementation for a variety of LRSM mass spectra, assuming flavour-democratic decays of heavy neutrinos, i.e. $\text{BR}(N \to e^+jj) = \text{BR}(N \to e^-jj) = \text{BR}(N \to \mu^+jj) = \text{BR}(N \to \mu^-jj) = 25\%$. Figure 8 displays the corresponding efficiencies obtained with Delphes for events in which two same-flavour leptons are reconstructed, showing their dependence on the Δ boson mass. Signal efficiencies decrease significantly at lower m_Δ, as fewer soft leptons satisfy isolation requirements. Also, as expected, final states containing muons exhibit slightly higher efficiencies due to the better muon reconstruction performance in the ATLAS detector parametrisation.

Figure 9 presents the projected sensitivities in the (m_Δ, m_N) plane for two benchmark values of the W_R boson mass: $M_{W_R} = 6$ TeV (left) and 30 TeV (right). The dominant production processes, $pp \to W^{\pm}\Delta$ (blue) and $pp \to Z\Delta$ (red), are considered for integrated luminosities of 300 fb^{-1} (solid) and 3000 fb^{-1} (shaded), corresponding to the expected luminosity of the Run 3 and high-luminosity phase of the LHC, respectively. The figures also display the heavy neutrino lifetime isolines. The sensitivity reach depends significantly on

JHEP06(2025)254

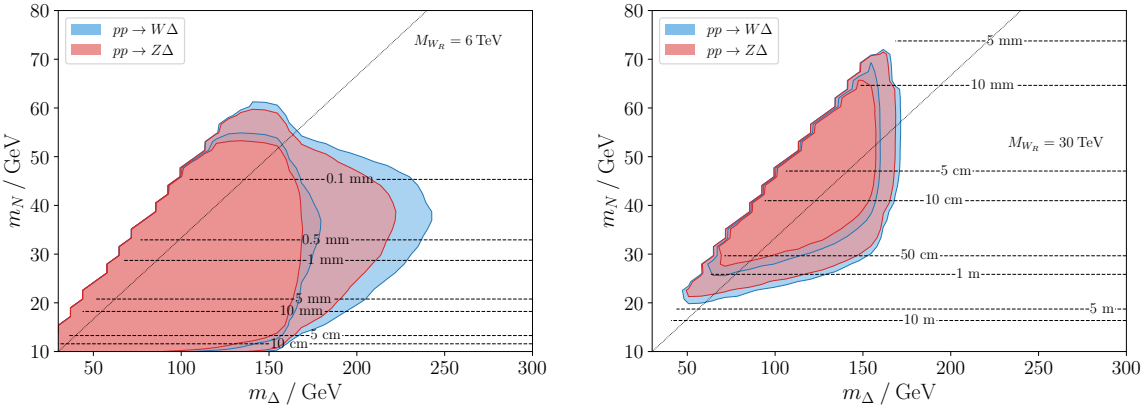


Figure 9. Sensitivity contours in the (m_Δ, m_N) plane for the $pp \to W^\pm\Delta$ (blue) and $pp \to Z\Delta$ Δ (red) production processes, with the inner (outer) contours corresponding to an integrated luminosity of 300 fb^{-1} (3000 fb^{-1}). The horizontal dashed lines indicate the proper lifetime of the heavy neutrino N, while the diagonal dotted line marks benchmark scenarios with $m_N = m_\Delta/3$. The left and right panels show results for $M_{W_R} = 6$ and 30 TeV, respectively.

M_{W_R}. For $M_{W_R} = 6$ TeV, the displacement is sizeable but remains within the detector size, allowing broad coverage in m_N and m_Δ up to approximately $m_N \simeq 70\,\text{GeV}$ and $m_\Delta \simeq 220\,\text{GeV}$. Beyond this mass range, the $\Delta \to NN$ decay becomes subdominant (see also figures 4 and 5) and sensitivity is lost. On the other hand, for a heavier W_R boson, the displacement of the heavy neutrino increases beyond the tracker volume, significantly reducing the accessible region of the parameter space. To further characterise the sensitivity, we consider the benchmark relation $m_\Delta = 3m_N$, which is represented by the diagonal line in the figure. This choice optimises the coverage in the (m_Δ, m_N) plane and enables us to quantitatively determine the indirect sensitivity to the W_R boson, and compare with conventional searches.

The resulting sensitivities, still based on $pp \to W^\pm\Delta$ and $pp \to Z\Delta$, are shown in figure 10. The left panel highlights the independent contributions from the Tracker Region (blue and red) and the Muon System Region (green and orange). Sensitivity extends up to $m_\Delta \simeq 180\,\text{GeV}$, beyond which the $\Delta \to ZZ$ decay becomes dominant, followed by the $\Delta \to hh$ mode (see figures 4 and 5), so that the signal cross section time branching ratio becomes negligible. The indirect sensitivity to the W_R boson mass reaches up to $M_{W_R} \simeq 70 - 80$ TeV, corresponding to an $\text{SU}(2)_R$-breaking scale of approximately $v_R \simeq \mathcal{O}(100\,\text{TeV})$ for N masses around $m_N \simeq 40 - 50\,\text{GeV}$. For lower m_N, the displacement increases beyond the tracker volume, and the muon system signal region becomes the dominant detection channel. This enables sensitivity for $m_N \simeq 10 - 20\,\text{GeV}$. Our results hence significantly surpass the current W_R bounds from direct di-jet searches (grey region), which are primarily constrained to lower W_R masses. This is emphasised in the right panel of figure 10, where we compare our projected reach with existing W_R limits not only from di-jet searches, but also from CMS and ATLAS searches for the KS process (pink and purple). Additionally, we show the projected reach for the KS process at a future 100 TeV circular collider (grey contour), as taken from [61]. This comparison highlights the importance of our proposed search strategy, which provides indirect access to W_R bosons much deeper in the multi-TeV range than any other search by means of soft and displaced objects.

JHEP06(2025)254

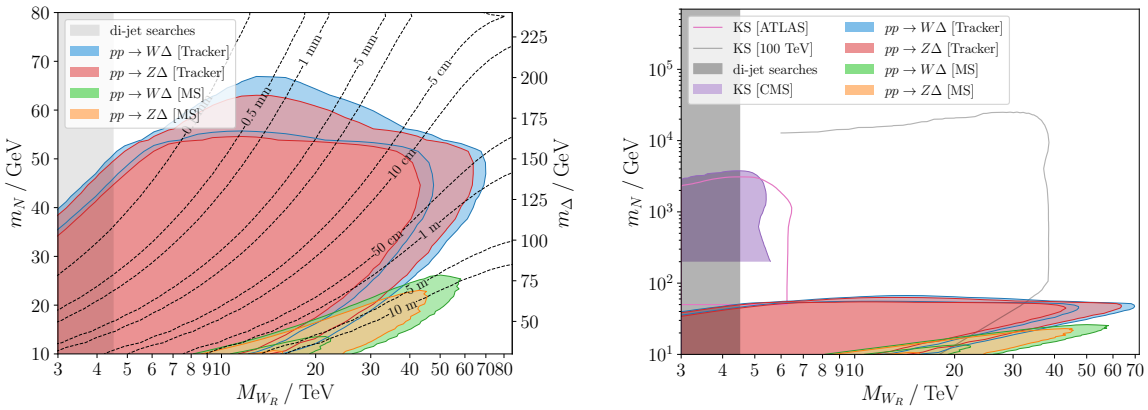


Figure 10. Sensitivity contours in the $(m_{W_R}, m_N = m_\Delta/3)$ plane as determined from Tracker Region analysis and Muon System (MS) Region analysis, and for the $pp \to W^\pm\Delta$ (blue and green) and $pp \to Z\Delta$ (red and orange) production processes. The dashed lines mark again the proper lifetime of the heavy neutrino N. Our results are compared, in the right panel, with the current reach of di-jet searches (grey region), existing ATLAS and CMS searches for the KS process (pink and purple), and the projected sensitivity at a future 100 TeV proton-proton collider.

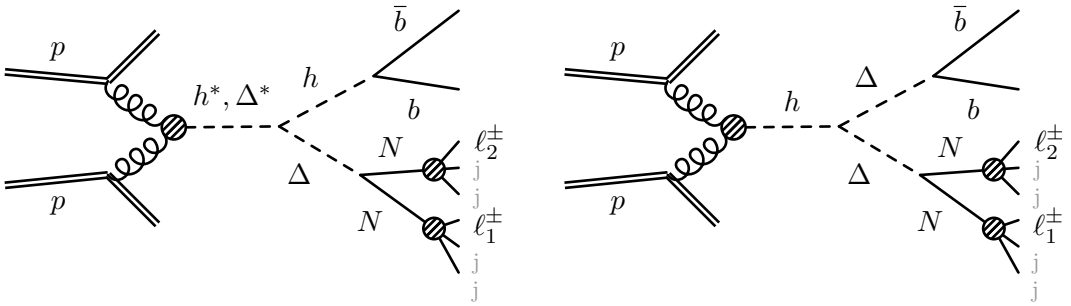


Figure 11. Representative Feynman diagrams for the production of beauty and Majorana neutrino pairs in the associated $pp \to h\Delta$ channel (left) and pair production $pp \to \Delta\Delta$ mode via mostly on-shell h-boson exchange (right).

5.2 The $b\bar{b}NN$ signature

In addition to the primary production channels of Δ discussed so far, we also considered in section 3.2 its pair production via a potentially resonant Higgs boson exchange, $gg \to h^{(*)} \to \Delta\Delta$, as well as its associated production with a Higgs boson, $gg \to h\Delta$. In this section, we focus on these two processes, with again a subsequent decay of the Δ state into heavy neutrinos, $\Delta \to NN$, followed by the decay $N \to \ell^\pm jj$. To maximise signal rates, we restrict our analysis of the associated production channel to cases where the Higgs boson decays into a pair of bottom quarks, $h \to b\bar{b}$. Similarly, for the pair production mode, we consider scenarios in which one Δ boson decays into heavy neutrinos, while the other decays into a $b\bar{b}$ pair, such a decay mode being mediated via the mixing of the Δ scalar with the SM Higgs boson. These production mechanisms, illustrated schematically by the diagrams of figure 11, present an intriguing opportunity to simultaneously probe the spontaneous mass generation

JHEP06(2025)254

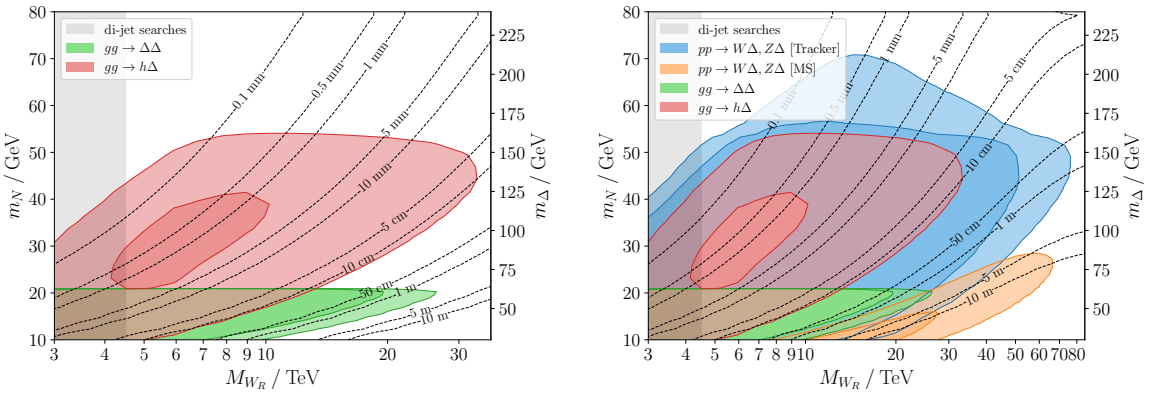


Figure 12. Sensitivity contours in the $(m_{W_R}, m_N = m_\Delta/3)$ plane for the $b\bar{b}NN$ signature (left panel), distinguishing the Δh associated production mode (red) and the $\Delta\Delta$ pair production mode (green). The inner(outer) contours correspond to an integrated luminosity of 300(3000 fb^{-1}). The dashed lines mark the lifetime of the heavy neutrino N, and the shaded grey region represents the exclusion from di-jet searches. In the right panel, we compare this reach to that originating from the study of Δ-strahlung processes in the Tracker (blue) and Muon System (orange).

of *Dirac particles* (through the final-state b-jets) and the spontaneous mass generation of *Majorana states* N. Moreover, if both production channels are observed, their relative signal strengths could provide a direct handle on the $h\Delta$ mixing angle.

For our analysis, we apply the same selection criteria as in section 5.1. Since the Higgs boson is significantly heavier than the weak bosons ($m_h > M_Z, M_W$), the production threshold and, consequently, the boost of the Δ state are larger than in the Δ-strahlung case previously studied. This subsequently results in greater lepton displacements, as discussed in section 4.2. The corresponding efficiencies, shown in figure 8 and table 3, confirm that these modes exhibit slightly higher efficiencies compared to the Δ-strahlung production channels. However, the Δ pair production via s-channel Higgs exchange is only sizeable if the intermediate Higgs boson can be resonantly produced ($m_\Delta < m_h/2$), limiting its coverage of the parameter space. Moreover, we emphasise that in this low-mass regime, the lepton isolation requirement rejects a significant fraction of events, leading to signal efficiencies of only $1\% - 5\%$ for $m_\Delta \in [30, 60]$ GeV.

Due to its comparatively lower production cross section (see figure 3), the sensitivity reach for the associated production channel $gg \to h\Delta$ is reduced relative to the two Δ-strahlung channels. In addition, the pair production mode is further suppressed by the two Δ branching ratios. We indeed recall that $\mathrm{BR}(\Delta \to b\bar{b}) > \mathrm{BR}(\Delta \to NN)$ in most of the relevant parameter space for $m_\Delta \leq m_h/2$, and that $\mathrm{BR}(\Delta \to NN)$ is small (see figures 4 and 5). Nevertheless, as will be shown, the $b\bar{b}NN$ final state remains a promising signature within the reach of the LHC, offering a complementary discovery channel alongside the Δ-strahlung processes studied in the previous section. This is quantified in figure 12, where we present projected sensitivities assuming integrated luminosities of 300 fb^{-1} (inner contours) and 3000 fb^{-1} (outer contours). The left panel displays both $b\bar{b}NN$ channels along with the proper lifetime of the heavy neutrino N. The reach for associated production mode (red contours) is found to extend up to $M_{W_R} \simeq 30$ TeV and $m_\Delta \simeq 160$ GeV. In contrast, the sensitivity for the

JHEP06(2025)254

pair production mode (green contours) decreases sharply as m_Δ approaches $m_h/2$, since the resonance enhancement is lost. However, in the resonant regime, the larger production cross section allows the reach to extend up to $M_{W_R} \simeq 25$ TeV. In the right panel of figure 12, we directly compare the sensitivity of the $b\bar{b}NN$ channels with the Δ-strahlung modes, combining the $pp \to W\Delta$ and $pp \to Z\Delta$ signals for displaced vertex searches in both the tracker (blue contour) and the muon system (orange contour). This figure highlights the complementarity of the different search strategies explored in this study, demonstrating that a comprehensive experimental programme can substantially extend the reach for minimal LRSM bosons deep in the multi-TeV regime.

6 Conclusion and outlook

Apart from low-energy probes such as neutrinoless double-beta decay or lepton-number violating meson decays, heavy Majorana neutrinos could, in principle, be produced at the LHC and lead to distinct lepton-number violating signatures with same-sign dileptons. The observation of such processes would then provide conclusive evidence for the Majorana nature of neutrinos. Furthermore, if the mass of heavy Majorana neutrinos N arises from spontaneous symmetry breaking, then a corresponding 'Majorana Higgs' boson Δ should exist as the source of their mass. Building on previous studies, we explored several production mechanisms for this Δ scalar, focusing on both its pair production via gluon fusion and its associated production with a SM W, Z, or Higgs boson. Through a detailed analytical analysis, we have demonstrated that a significant number of events could be expected in the datasets of the upcoming LHC runs, highlighting promising avenues for discovery.

We frame our study within the minimal left-right symmetric model as an illustrative UV-complete framework to explore the potential signatures arising from Δ production and decay at colliders. We have considered a $\Delta \to NN$ final state, where the neutrino N is long-lived so that its decay leads to displaced vertex signatures in typical LHC detectors. As in the left-right framework, the N lifetime is primarily governed by the heavy neutrino mass and the $\mathrm{SU}(2)_R$ breaking scale, and therefore the mass of the heavy W_R gauge boson, exploiting N reconstruction either in the tracker or in the muon system of a detector grants access to regimes of very large W_R masses. We obtain an indirect sensitivity reaching $M_{W_R} \simeq 70 - 80\,\mathrm{TeV}$, effectively turning the LHC into a precision probe of left-right symmetry breaking. This reach surpasses the expected sensitivity of direct heavy neutrino searches via the KS mechanism at a future pp collider operating at $\sqrt{s} = 100$ TeV, which is limited to $M_{W_R} \simeq (20)\,40$ TeV for $m_N \simeq (10)\,1000\,\mathrm{GeV}$. The processes that we explored thus probe a complementary portion of the LRSM parameter space, and could serve as a powerful indirect discovery tool potentially guiding future searches for heavy resonances via the KS mechanism. In addition, we have also examined associated Δ production with a SM Higgs boson decaying into a $b\bar{b}$ pair. The resulting signature comprising two b-jets and two long-lived heavy neutrinos then offers the exciting possibility to simultaneously establish the spontaneous mass origin of *Dirac fermions* and *Majorana states*, although the sensitivity expressed in terms of the W_R boson mass is comparatively lower.

Our analyses could be further improved by including the $pp \to t\bar{t}\Delta$ production channel with cross sections lying typically one order of magnitude below the one expected for Δ-

JHEP06(2025)254

strahlung. Another foreseeable improvement would be to also consider semi-visible final states where one heavy neutrino N decays inside the inner detector while the other one escapes detection. Additionally, Δ pair production yields a $\Delta L = 4$ signature via $gg \to \Delta\Delta \to 4N$ decays, whose observation and low rate could be related to $0\nu4\beta$ decay processes [94, 95]. If the Δ mass is large enough to allow for decays into pairs of W, Z, or Higgs bosons, the lepton-number violating signal yield considered in this study drastically decreases, correspondingly opening the door to searches for heavier Δ states through (partially) resonant multi-boson final states. Moreover, if the mixing between the SM Higgs boson and the Δ scalar is below approximately 1%, the Δ-strahlung production modes become highly suppressed. In this regime, Δ decays into the NN final state however still largely dominate so that the resulting signals could be probed at a future (very) high-energy hadron collider through the process $pp \to W_R\Delta$. Depending on the decay mode of the W_R boson, this channel could lead to an intriguing $\Delta L = 4$ final state, providing a rare and striking signature of lepton number violation at unprecedented energy scales.

Acknowledgments

JK and MN are supported by the Slovenian Research Agency under the research core funding No. P1-0035 and in part by the research grants J1-3013 and N1-0253, while the work of BF has been partly supported by Grant ANR-21-CE31-0013 (project DMwithLLPatLHC) from the French *Agence Nationale de la Recherche*. The work of BF, JK and MN has received further support by the bilateral project Proteus PR-12696/Projet 50194VC.

A Box amplitudes for $gg \to S_1S_2$

The amplitude in eq. (3.6) receives contributions from both triangle and box diagrams with an internal quark loop. We present below expressions for the box contributions, split in several parts according to the permutation of external momenta for clarity. The contributions to the box amplitudes can be written as

$$\mathcal{M}_{\square}^{00} = i\sum_q Y_{S_1}^q Y_{S_2}^q \Big(\mathcal{F}_{\square}^1(\hat{s},\hat{t},\hat{u}) + \mathcal{F}_{\square}^1(\hat{s},\hat{u},\hat{t}) + \mathcal{G}_{\square}^1(\hat{s},\hat{t},\hat{u})\Big)\,, \tag{A.1}$$

$$\mathcal{M}_{\square}^{21} = i\sum_q Y_{S_1}^q Y_{S_2}^q \Big(\mathcal{F}_{\square}^2(\hat{s},\hat{t},\hat{u}) + \mathcal{F}_{\square}^2(\hat{s},\hat{u},\hat{t}) + \mathcal{G}_{\square}^2(\hat{s},\hat{t},\hat{u})\Big)\,, \tag{A.2}$$

$$\mathcal{M}_{\square}^{31} = i\sum_q Y_{S_1}^q Y_{S_2}^q \Big(\mathcal{F}_{\square}^3(\hat{s},\hat{t},\hat{u}) + \mathcal{F}_{\square}^4(\hat{s},\hat{u},\hat{t}) + \mathcal{G}_{\square}^3(\hat{s},\hat{t},\hat{u})\Big)\,, \tag{A.3}$$

$$\mathcal{M}_{\square}^{23} = i\sum_q Y_{S_1}^q Y_{S_2}^q \Big(\mathcal{F}_{\square}^4(\hat{s},\hat{t},\hat{u}) + \mathcal{F}_{\square}^3(\hat{s},\hat{u},\hat{t}) + \mathcal{G}_{\square}^4(\hat{s},\hat{t},\hat{u})\Big)\,, \tag{A.4}$$

where the Yukawa couplings are $\frac{1}{\cos\theta}Y_h^q \approx \frac{1}{\sin\theta}Y_\Delta^q \approx \frac{m_q}{v}$ and the loop-functions are

$$\begin{aligned}\mathcal{F}_{\square}^1(x,y,z) = -4(B_0(x)+B_0(y)) - 2\Big(&xC_0(0,0,x) + (m_{S_1}^2 - x - z)C_0(0,m_{S_2}^2,y)\\ &- (m_{S_1}^2 - y)C_0(0,m_{S_1}^2,y) + (8m_q^2 - y - z)C_0(m_{S_1}^2,m_{S_2}^2,x) - 8C_{00}(0,x,0)\\ &+ x(4m_q^2 - y)D_0 - 4(8m_q^2 - y - z)D_{00}\Big)\,,\end{aligned} \tag{A.5}$$

JHEP06(2025)254

$$\mathcal{F}^2_{\Box}(x,y,z) = -4\Big(C_0(0,m^2_{S_2},y) + 2C_2(0,m^2_{S_2},y) + 4C_{12}(0,x,0) - C_0(0,x,0) + (y-4m_q^2)D_0 - (m^2_{S_1}-y)(D_1+D_2) + (m^2_{S_1}-z)D_3 + 2(8m_q^2-y-z)(D_{13}+D_{23})\Big)\,, \tag{A.6}$$

$$\mathcal{F}^3_{\Box}(x,y,z) = -4\Big(C_0(m^2_{S_1},m^2_{S_2},x) + C_0(y,m^2_{S_1},0) - 2C_1(y,m^2_{S_2},0) + x(D_1+D_2) + 2(8m_q^2-y-z)(D_{12}+D_{22}) + (m^2_{S_1}-z)D_2\Big)\,, \tag{A.7}$$

$$\mathcal{F}^4_{\Box}(x,y,z) = 4\Big(C_0(m^2_{S_1},m^2_{S_2},x) + C_0(0,m^2_{S_2},y) + 2C_1(y,m^2_{S_2},0) + 2(8m_q^2-y-z)D_{23} + xD_3 + (y-m^2_{S_1})D_2\Big)\,. \tag{A.8}$$

The quantities $D_{ij} \equiv D_{ij}(0,m^2_{S_1},m^2_{S_2},0,y,x)$, and we further abbreviate the Passarino-Veltman scalar integrals as

$$B_0(x_1) \equiv B_0(x_1,m_q^2,m_q^2) \tag{A.9}$$

$$C_{ij}(x_1,x_2,x_3) \equiv C_{ij}(x_1,x_2,x_3,m_q^2,m_q^2,m_q^2) \tag{A.10}$$

$$D_{ij}(x_1,x_2,x_3,x_4,x_5,x_6) \equiv D_{ij}(x_1,x_2,x_3,x_4,x_5,x_6,m_q^2,m_q^2,m_q^2,m_q^2)\,, \tag{A.11}$$

consistent with the convention and notation of LoopTools [74]. We further have

$$\mathcal{G}^1_{\Box}(x,y,z) = 4(B_0(y)+B_0(z)) - 2\Big((m^2_{S_1}-z)(C_0(0,z,m^2_{S_1})-C_0(0,m^2_{S_2},y)) + (m^2_{S_1}-y)(C_0(y,0,m^2_{S_1})-C_0(m^2_{S_2},0,z)) + x(C_0(0,m^2_{S_2},y)+C_0(m^2_{S_2},0,z)) + x(4m_q^2-m^2_{S_1})D_0 + (m^2_{S_1}-y)(m^2_{S_1}-z)D_0 - 4(8m_q^2-y-z)D_{00}\Big) \tag{A.12}$$

$$\mathcal{G}^2_{\Box}(x,y,z) = 4\Big(C_0(0,m^2_{S_2},y) - C_0(m^2_{S_2},0,z) + 2C_2(0,m^2_{S_2},y) - 2(C_1(m^2_{S_2},0,z)+C_2(m^2_{S_2},0,z)) + (z-m^2_{S_1})D_3 + (y-m^2_{S_1})D_2 + (4m_q^2-m^2_{S_1})D_0 + 2(y+z-8m_q^2)D_{23}\Big)\,, \tag{A.13}$$

$$\mathcal{G}^3_{\Box}(x,y,z) = 4\Big(C_0(y,0,m^2_{S_1}) + C_0(m^2_{S_2},0,z) + 2C_1(m^2_{S_2},0,z) + 2C_2(m^2_{S_2},0,z) - 2C_2(0,m^2_{S_2},y) + (x+2y+3z-m^2_{S_1}-16m_q^2)D_2 + (z-m^2_{S_1})D_1 + 2(y+z-8m_q^2)(D_{12}+D_{22})\Big)\,, \tag{A.14}$$

$$\mathcal{G}^4_{\Box}(x,y,z) = 4\Big(C_0(0,z,m^2_{S_1}) - C_0(0,m^2_{S_2},y) + 2C_0(m^2_{S_2},0,z) + 2C_1(m^2_{S_2},0,z) + 2C_2(m^2_{S_2},0,z) - 2C_2(0,m^2_{S_2},y) + (m^2_{S_1}-y)(D_0+D_1+D_2) + xD_3 + 2(8m_q^2-y-z)(D_{13}+D_{23})\Big)\,, \tag{A.15}$$

with this time $D_{ij} \equiv D_{ij}(m^2_{S_1},0,m^2_{S_2},0,y,z)$. In order to bring the amplitudes to this compact form we have used the following symmetry relations of the Passarino-Veltman functions

$$C_0(x,y,z) = C_0(x,z,y) = C_0(z,y,x) + \text{ cyclic perm.}\,, \tag{A.16}$$

$$C_1(x,y,z) = C_2(z,y,x)\,, \tag{A.17}$$

$$D_{0,2,00,13,22}(a,b,c,d,x,y) = D_{0,2,00,13,22}(d,c,b,a,x,y)\,, \tag{A.18}$$

JHEP06(2025)254

$$D_1(a,b,c,d,x,y) = D_3(d,c,b,a,x,y)\,, \tag{A.19}$$
$$D_{12}(a,b,c,d,x,y) = D_{23}(d,c,b,a,x,y)\,, \tag{A.20}$$
$$D_{11}(a,b,c,d,x,y) = D_{33}(d,c,b,a,x,y)\,, \tag{A.21}$$

which hold for coinciding internal masses (or propagator poles), as in eqs. (A.9)–(A.11).

B Phase space integration

The differential cross sections derived in this work are numerically integrated over the phase space with a Monte Carlo method such as the VEGAS algorithm [96, 97]. Moreover, PDF values are obtained with the Python interface of LHAPDF 6.5.4 [76]. For better numerical stability and in order to derive distributions, it is convenient to change the integration variables from the Bjorken variables $x_{1,2}$ to the reduced invariant mass $\tau = m_{\text{inv}}/s$ and rapidity y

$$\begin{aligned} &x_{1,2} = \sqrt{\tau}\exp(\pm y)\,, \qquad \tau = x_1 x_2\,, \qquad y = \frac{1}{2}\log\left(x_1/x_2\right)\,, \qquad \mathrm{d}x_1\mathrm{d}x_2 = \mathrm{d}\tau\mathrm{d}y\,, \\ &\tau \in \left[\frac{(m_1+m_2)^2}{s}, 1\right]\,, \qquad y \in \left[-\log\left(\frac{1}{\sqrt{\tau}}\right), \log\left(\frac{1}{\sqrt{\tau}}\right)\right]\,. \end{aligned} \tag{B.1}$$

Depending on the mass configuration of the final state scalars of masses m_1 and m_2, their production can be enhanced via massive s-channel resonant exchanges (e.g. the triangle diagrams in $gg \to h \to \Delta\Delta$), leading to a sharply peaked integrand in the variable τ. This poses a problem for Monte Carlo integrators, and it is thus convenient to change the integration variables to flatten the pole in the τ direction and precondition the integrator to ensure smooth sampling around the pole. Assuming a single resonance, the pole structure admits a Breit-Wigner shape

$$\mathrm{BW}(\tau) \simeq \frac{1}{((\tau s - M_R^2)^2 + \Gamma_R^2 M_R^2}\,, \tag{B.2}$$

where M_R and Γ_R are the real and imaginary parts of the propagator pole of the resonance R, that is in this case the mass and the total width of the s-channel mediator. The integration variable τ can then be transformed symmetrically around the resonance as

$$\begin{aligned} &\tau(u) = \frac{M_R^2}{s} + \frac{\Gamma_R M_R}{s}\tan\left[\pi\left(u - \frac{1}{2}\right)\right]\,, \qquad \frac{\mathrm{d}\tau}{\mathrm{d}u} = \pi\frac{\Gamma_R M_R}{s\cos^2\left(\pi(u-1/2)\right)}\,, \\ &u_{\text{min/max}} = \frac{1}{2} + \frac{1}{\pi}\arctan\left(\frac{s\,\tau_{\text{min/max}} - M_R^2}{\Gamma_R M_R}\right)\,. \end{aligned} \tag{B.3}$$

For numerical computations, the Higgs boson width has been fixed to the central value returned by current measurements, $\Gamma_{\text{tot}}(h) = 3.7^{+1.9}_{-1.4}\,\text{MeV}$ [98]. A smaller (larger) value would lead to a significant increase (decrease) of the $gg \to h \to \Delta\Delta$ cross section, as shown in figure 13 where we vary the Higgs width within the current 1σ band. The resulting variation is found to be significant only in the resonant regime, as expected.

JHEP06(2025)254

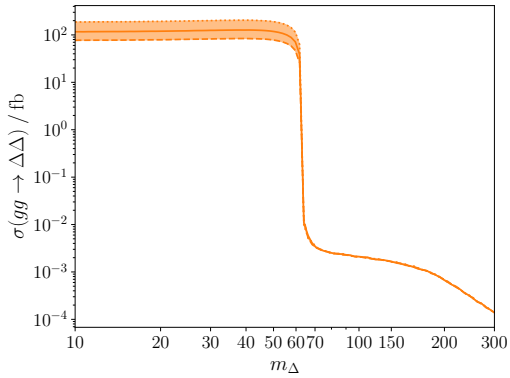


Figure 13. Variation of the $gg \to \Delta\Delta$ production cross section with respect to m_Δ and the Higgs-width $\Gamma_{\text{tot}}(h)$. The solid line denotes the central value $\Gamma(h) = 3.7\,\text{MeV}$, while the envelope spanned by dashed (dotted) lines denotes $\Gamma(h) = 5.6\,\text{MeV}$ ($\Gamma(h) = 2.3\,\text{MeV}$).

C Efficiency tables

In this appendix we present signal efficiencies resulting from the isolation requirements and reconstruction performance outlined in section 5. Selected events include exactly two reconstructed leptons with $p_T(\ell) > 10\,\text{GeV}$, $|\eta(\ell)| < 2.4$ and are well isolated from the closest jet j_c with $\Delta R(\ell, j_c) > 0.4$.

JHEP06(2025)254

$pp \to h\Delta \to b\bar{b}\,NN$		e^+e^-	$\mu^+\mu^-$	$e^\pm\mu^\mp$	$e^\pm e^\pm$	$\mu^\pm\mu^\pm$	$e^\pm\mu^\pm$
$m_\Delta = 50\,\text{GeV}$	Prompt	0.2%	0.2%	0.5%	0.1%	0.2%	0.4%
	Long-lived	4.6%	4.7%	9.7%	4.2%	4.6%	9.4%
$m_\Delta = 100\,\text{GeV}$	Prompt	2.0%	1.9%	3.8%	2.0%	1.8%	3.2%
	Long-lived	2.6%	2.4%	4.8%	2.3%	2.3%	5.0%
$m_\Delta = 150\,\text{GeV}$	Prompt	5.9%	5.8%	12.0%	5.7%	6.1%	10.8%
	Long-lived	0.6%	0.4%	0.8%	0.4%	0.3%	0.8%
$m_\Delta = 200\,\text{GeV}$	Prompt	6.6%	7.0%	13.9%	6.5%	6.8%	14.2%
	Long-lived	0.4%	0.3%	0.5%	0.1%	0.1%	0.1%
$m_\Delta = 250\,\text{GeV}$	Prompt	6.8%	6.6%	12.6%	6.2%	6.6%	13.2%
	Long-lived	0.3%	0.2%	0.6%	0.2%	0.1%	0.2%
$pp \to Z\Delta \to b\bar{b}\,NN$		e^+e^-	$\mu^+\mu^-$	$e^\pm\mu^\mp$	$e^\pm e^\pm$	$\mu^\pm\mu^\pm$	$e^\pm\mu^\pm$
$m_\Delta = 50\,\text{GeV}$	Prompt	0.1%	0.1%	0.1%	0.1%	–	0.1%
	Long-lived	1.1%	1.1%	2.5%	1.3%	1.2%	2.3%
$m_\Delta = 100\,\text{GeV}$	Prompt	1.2%	1.1%	2.3%	1.1%	1.1%	2.4%
	Long-lived	1.2%	1.3%	2.1%	1.1%	1.1%	2.4%
$m_\Delta = 150\,\text{GeV}$	Prompt	4.5%	5.1%	9.3%	4.4%	4.5%	8.9%
	Long-lived	0.3%	0.2%	0.5%	0.2%	0.2%	0.3%
$m_\Delta = 200\,\text{GeV}$	Prompt	6.3%	6.7%	12.6%	5.8%	6.2%	12.5%
	Long-lived	0.2%	0.1%	0.3%	0.1%	–	0.2%
$m_\Delta = 250\,\text{GeV}$	Prompt	5.7%	6.0%	11.5%	6.2%	5.4%	11.9%
	Long-lived	0.3%	0.2%	0.4%	–	0.1%	0.2%
$pp \to W\Delta \to jj\,NN$		e^+e^-	$\mu^+\mu^-$	$e^\pm\mu^\mp$	$e^\pm e^\pm$	$\mu^\pm\mu^\pm$	$e^\pm\mu^\pm$
$m_\Delta = 50\,\text{GeV}$	Prompt	–	–	–	–	–	–
	Long-lived	1.1%	0.9%	1.8%	1.0%	0.8%	1.9%
$m_\Delta = 100\,\text{GeV}$	Prompt	0.9%	1.0%	2.0%	0.9%	0.9%	1.9%
	Long-lived	0.8%	0.9%	1.8%	0.7%	0.7%	1.6%
$m_\Delta = 150\,\text{GeV}$	Prompt	4.6%	4.5%	9.6%	4.4%	4.8%	8.8%
	Long-lived	0.1%	0.1%	0.1%	–	–	0.1%
$m_\Delta = 200\,\text{GeV}$	Prompt	6.7%	6.5%	12.7%	5.8%	7.0%	12.7%
	Long-lived	–	–	–	–	–	–
$m_\Delta = 250\,\text{GeV}$	Prompt	6.0%	6.3%	12.0%	6.2%	6.3%	11.7%
	Long-lived	–	–	–	–	–	–

Table 1. Selection efficiencies when requiring two isolated leptons with $p_T > 10\,\text{GeV}$, $|\eta| < 2.4$, and either $|d_0| > 0.1$ mm (long-lived) or $|d_0| < 0.1$ mm (prompt). We consider signals emerging from $pp \to h\Delta \to b\bar{b}NN$ (upper), $pp \to Z\Delta \to b\bar{b}NN$ (middle) and $pp \to W\Delta \to jjNN$ (lower), for a scenario where $M_{W_R} = 6\,\text{TeV}$ and the heavy N decays democratically into electrons and muons. Leptons are required to be isolated from any jet by $\Delta R > 0.4$.

JHEP06(2025)254

$pp \to h\Delta \to b\bar{b}\,NN$		e^+e^-	$\mu^+\mu^-$	$e^\pm\mu^\mp$	$e^\pm e^\pm$	$\mu^\pm\mu^\pm$	$e^\pm\mu^\pm$
$m_\Delta = 50\,\text{GeV}$	Prompt	0.1%	0.2%	0.3%	0.1%	0.1%	0.1%
	Long-lived	4.9%	5.3%	10.1%	5.0%	4.8%	9.8%
$m_\Delta = 100\,\text{GeV}$	Prompt	0.3%	0.2%	0.3%	0.1%	0.1%	0.1%
	Long-lived	5.7%	5.9%	11.3%	5.4%	5.4%	10.1%
$m_\Delta = 150\,\text{GeV}$	Prompt	0.3%	0.2%	0.4%	0.1%	0.1%	0.4%
	Long-lived	5.9%	6.3%	12.7%	5.8%	6.6%	11.8%
$m_\Delta = 200\,\text{GeV}$	Prompt	0.6%	0.4%	0.7%	0.3%	0.3%	0.6%
	Long-lived	5.8%	6.2%	12.5%	6.0%	6.4%	11.8%
$m_\Delta = 250\,\text{GeV}$	Prompt	0.7%	0.6%	1.5%	0.6%	0.6%	1.3%
	Long-lived	5.0%	4.9%	10.0%	4.8%	5.5%	9.7%
$pp \to Z\Delta \to b\bar{b}\,NN$		e^+e^-	$\mu^+\mu^-$	$e^\pm\mu^\mp$	$e^\pm e^\pm$	$\mu^\pm\mu^\pm$	$e^\pm\mu^\pm$
$m_\Delta = 50\,\text{GeV}$	Prompt	0.1%	–	0.1%	–	–	–
	Long-lived	1.3%	1.5%	2.5%	1.1%	1.3%	2.5%
$m_\Delta = 100\,\text{GeV}$	Prompt	0.1%	–	–	–	–	–
	Long-lived	3.5%	3.3%	7.0%	3.5%	3.5%	6.8%
$m_\Delta = 150\,\text{GeV}$	Prompt	0.1%	0.1%	0.2%	0.1%	0.1%	0.1%
	Long-lived	5.1%	5.1%	9.4%	5.3%	4.9%	9.7%
$m_\Delta = 200\,\text{GeV}$	Prompt	0.3%	0.2%	0.6%	0.3%	0.2%	0.4%
	Long-lived	5.3%	5.2%	11.4%	5.1%	5.4%	10.9%
$m_\Delta = 250\,\text{GeV}$	Prompt	0.7%	0.6%	1.2%	0.5%	0.4%	1.2%
	Long-lived	4.5%	4.8%	9.1%	4.1%	4.4%	8.6%
$pp \to W\Delta \to jj\,NN$		e^+e^-	$\mu^+\mu^-$	$e^\pm\mu^\mp$	$e^\pm e^\pm$	$\mu^\pm\mu^\pm$	$e^\pm\mu^\pm$
$m_\Delta = 50\,\text{GeV}$	Prompt	–	–	–	–	–	–
	Long-lived	1.1%	1.1%	2.4%	0.8%	1.1%	2.2%
$m_\Delta = 100\,\text{GeV}$	Prompt	–	–	–	–	–	–
	Long-lived	3.4%	3.5%	6.8%	3.3%	3.3%	6.5%
$m_\Delta = 150\,\text{GeV}$	Prompt	0.1%	–	0.1%	–	–	–
	Long-lived	4.5%	5.0%	10.6%	5.1%	4.4%	9.6%
$m_\Delta = 200\,\text{GeV}$	Prompt	0.2%	0.1%	0.2%	–	0.1%	0.1%
	Long-lived	5.2%	5.7%	11.5%	5.2%	5.7%	11.0%
$m_\Delta = 250\,\text{GeV}$	Prompt	0.3%	0.3%	0.5%	0.2%	0.2%	0.5%
	Long-lived	4.6%	4.5%	9.0%	4.5%	4.5%	8.7%

Table 2. Selection efficiencies when requiring two isolated leptons with $p_T > 10\,\text{GeV}$, $|\eta| < 2.4$, and either $|d_0| > 0.1$ mm (long-lived) or $|d_0| < 0.1$ mm (prompt). We consider signals emerging from $pp \to h\Delta \to b\bar{b}NN$ (upper), $pp \to Z\Delta \to b\bar{b}NN$ (middle) and $pp \to W\Delta \to jjNN$ (lower), for a scenario where $M_{W_R} = 30\,\text{TeV}$ and the heavy N decays democratically into electrons and muons. Leptons are required to be isolated from any jet by $\Delta R > 0.4$.

JHEP06(2025)254

$pp \to \Delta\Delta \to bb\,NN$		e^+e^-	$\mu^+\mu^-$	$e^\pm\mu^\mp$	$e^\pm e^\pm$	$\mu^\pm\mu^\pm$	$e^\pm\mu^\pm$
$m_\Delta = 50\,\text{GeV}$	Prompt	0.1%	0.1%	–	0.1%	–	–
	Long-lived	1.1%	1.0%	2.0%	1.0%	1.0%	2.0%
$m_\Delta = 100\,\text{GeV}$	Prompt	1.9%	2.0%	3.9%	2.0%	1.9%	3.9%
	Long-lived	2.8%	2.4%	5.7%	2.1%	2.3%	4.9%
$m_\Delta = 150\,\text{GeV}$	Prompt	5.8%	5.3%	11.7%	5.4%	5.5%	11.2%
	Long-lived	0.5%	0.5%	1.1%	0.2%	0.4%	0.8%
$m_\Delta = 200\,\text{GeV}$	Prompt	7.4%	7.3%	13.9%	6.8%	6.8%	13.2%
	Long-lived	0.4%	0.4%	0.7%	0.1%	0.1%	0.3%
$m_\Delta = 250\,\text{GeV}$	Prompt	6.8%	6.6%	13.3%	6.2%	6.6%	13.1%
	Long-lived	0.5%	0.5%	0.9%	0.2%	0.1%	0.3%

$pp \to \Delta\Delta \to b\bar{b}\,NN$		e^+e^-	$\mu^+\mu^-$	$e^\pm\mu^\mp$	$e^\pm e^\pm$	$\mu^\pm\mu^\pm$	$e^\pm\mu^\pm$
$m_\Delta = 50\,\text{GeV}$	Prompt	–	–	–	–	–	–
	Long-lived	1.1%	1.2%	2.5%	1.1%	1.2%	2.2%
$m_\Delta = 100\,\text{GeV}$	Prompt	0.3%	0.2%	0.4%	0.1%	–	0.1%
	Long-lived	5.7%	5.8%	11.1%	5.5%	5.4%	11.1%
$m_\Delta = 150\,\text{GeV}$	Prompt	0.4%	0.2%	0.5%	0.1%	0.1%	0.3%
	Long-lived	6.2%	5.9%	12.1%	5.9%	6.3%	10.8%
$m_\Delta = 200\,\text{GeV}$	Prompt	0.5%	0.3%	0.7%	0.3%	0.3%	0.6%
	Long-lived	6.7%	6.7%	12.4%	5.9%	5.7%	12.3%
$m_\Delta = 250\,\text{GeV}$	Prompt	0.9%	0.7%	1.6%	0.8%	0.6%	1.3%
	Long-lived	5.1%	5.2%	10.0%	4.8%	4.8%	9.9%

Table 3. Same as table 2, but for $pp \to \Delta\Delta \to b\bar{b}NN$, and for a scenario where $M_{W_R} = 6\,\text{TeV}$ (upper) and $M_{W_R} = 30\,\text{TeV}$ (lower).

JHEP06(2025)254

Data Availability Statement. This article has no associated data or the data will not be deposited.

Code Availability Statement. This article has no associated code or the code will not be deposited.

Open Access. This article is distributed under the terms of the Creative Commons Attribution License (CC-BY4.0), which permits any use, distribution and reproduction in any medium, provided the original author(s) and source are credited.

References

[1] P. Minkowski, $\mu \to e\gamma$ *at a Rate of One Out of* 10^9 *Muon Decays?*, *Phys. Lett. B* **67** (1977) 421 [INSPIRE].

[2] M. Gell-Mann, P. Ramond and R. Slansky, *Complex Spinors and Unified Theories*, *Conf. Proc. C* **790927** (1979) 315 [arXiv:1306.4669] [INSPIRE].

[3] S.L. Glashow, *The Future of Elementary Particle Physics*, *NATO Sci. Ser. B* **61** (1980) 687 [INSPIRE].

[4] R.N. Mohapatra and G. Senjanović, *Neutrino Mass and Spontaneous Parity Nonconservation*, *Phys. Rev. Lett.* **44** (1980) 912 [INSPIRE].

[5] T. Yanagida, *Horizontal gauge symmetry and masses of neutrinos* in the proceedings of the *Workshop on the Unified Theories and the Baryon Number in the Universe* Tsukuba, Japan, February 13–14 (1979) [INSPIRE].

[6] J.C. Pati and A. Salam, *Lepton Number as the Fourth Color*, *Phys. Rev. D* **10** (1974) 275 [INSPIRE].

[7] R.N. Mohapatra and J.C. Pati, *A Natural Left-Right Symmetry*, *Phys. Rev. D* **11** (1975) 2558 [INSPIRE].

[8] G. Senjanović, *Spontaneous Breakdown of Parity in a Class of Gauge Theories*, *Nucl. Phys. B* **153** (1979) 334 [INSPIRE].

[9] A. Maiezza, M. Nemevšek, F. Nesti and G. Senjanović, *Left-Right Symmetry at LHC*, *Phys. Rev. D* **82** (2010) 055022 [arXiv:1005.5160] [INSPIRE].

[10] G. Beall, M. Bander and A. Soni, *Constraint on the Mass Scale of a Left-Right Symmetric Electroweak Theory from the* $K_L - K_S$ *Mass Difference*, *Phys. Rev. Lett.* **48** (1982) 848 [INSPIRE].

[11] G. Senjanović and P. Senjanović, *Suppression of Higgs Strangeness Changing Neutral Currents in a Class of Gauge Theories*, *Phys. Rev. D* **21** (1980) 3253 [INSPIRE].

[12] Y. Zhang, H. An, X. Ji and R.N. Mohapatra, *General CP Violation in Minimal Left-Right Symmetric Model and Constraints on the Right-Handed Scale*, *Nucl. Phys. B* **802** (2008) 247 [arXiv:0712.4218] [INSPIRE].

[13] S. Bertolini, A. Maiezza and F. Nesti, *Present and Future K and B Meson Mixing Constraints on TeV Scale Left-Right Symmetry*, *Phys. Rev. D* **89** (2014) 095028 [arXiv:1403.7112] [INSPIRE].

[14] G. Ecker and W. Grimus, *CP violation and left-right symmetry*, *Nucl. Phys. B* **258** (1985) 328 [INSPIRE].

JHEP06(2025)254

[15] K. Kiers et al., *Ubiquitous CP violation in a top inspired left-right model*, *Phys. Rev. D* **66** (2002) 095002 [hep-ph/0205082] [INSPIRE].

[16] A. Maiezza and M. Nemevšek, *Strong P invariance, neutron electric dipole moment, and minimal left-right parity at LHC*, *Phys. Rev. D* **90** (2014) 095002 [arXiv:1407.3678] [INSPIRE].

[17] S. Bertolini, A. Maiezza and F. Nesti, *Kaon CP violation and neutron EDM in the minimal left-right symmetric model*, *Phys. Rev. D* **101** (2020) 035036 [arXiv:1911.09472] [INSPIRE].

[18] R. Kuchimanchi, *Leptonic CP problem in left-right symmetric model*, *Phys. Rev. D* **91** (2015) 071901 [arXiv:1408.6382] [INSPIRE].

[19] G. Senjanović and V. Tello, *Strong CP violation: Problem or blessing?*, *Int. J. Mod. Phys. A* **38** (2023) 2350067 [arXiv:2004.04036] [INSPIRE].

[20] F. Bezrukov, H. Hettmansperger and M. Lindner, *keV sterile neutrino Dark Matter in gauge extensions of the Standard Model*, *Phys. Rev. D* **81** (2010) 085032 [arXiv:0912.4415] [INSPIRE].

[21] M. Nemevšek, G. Senjanović and Y. Zhang, *Warm Dark Matter in Low Scale Left-Right Theory*, *JCAP* **07** (2012) 006 [arXiv:1205.0844] [INSPIRE].

[22] M. Nemevšek and Y. Zhang, *Dark Matter Dilution Mechanism through the Lens of Large-Scale Structure*, *Phys. Rev. Lett.* **130** (2023) 121002 [arXiv:2206.11293] [INSPIRE].

[23] M. Nemevšek and Y. Zhang, *Anatomy of diluted dark matter in the minimal left-right symmetric model*, *Phys. Rev. D* **109** (2024) 056021 [arXiv:2312.00129] [INSPIRE].

[24] P.S.B. Dev, J. Heeck and A. Thapa, *Decaying scalar dark matter in the minimal left-right symmetric model*, arXiv:2501.14669 [INSPIRE].

[25] R.N. Mohapatra and G. Senjanović, *Neutrino Masses and Mixings in Gauge Models with Spontaneous Parity Violation*, *Phys. Rev. D* **23** (1981) 165 [INSPIRE].

[26] M. Nemevšek, G. Senjanović and V. Tello, *Connecting Dirac and Majorana Neutrino Mass Matrices in the Minimal Left-Right Symmetric Model*, *Phys. Rev. Lett.* **110** (2013) 151802 [arXiv:1211.2837] [INSPIRE].

[27] J. Kriewald, M. Nemevšek and F. Nesti, *Enabling precise predictions for left-right symmetry at colliders*, *Eur. Phys. J. C* **84** (2024) 1306 [arXiv:2403.07756] [INSPIRE].

[28] S. Weinberg, *A Model of Leptons*, *Phys. Rev. Lett.* **19** (1967) 1264 [INSPIRE].

[29] ATLAS collaboration, *A detailed map of Higgs boson interactions by the ATLAS experiment ten years after the discovery*, *Nature* **607** (2022) 52 [*Erratum ibid.* **612** (2022) E24] [arXiv:2207.00092] [INSPIRE].

[30] CMS collaboration, *A portrait of the Higgs boson by the CMS experiment ten years after the discovery*, *Nature* **607** (2022) 60 [arXiv:2207.00043] [INSPIRE].

[31] A. Maiezza, M. Nemevšek and F. Nesti, *Lepton Number Violation in Higgs Decay at LHC*, *Phys. Rev. Lett.* **115** (2015) 081802 [arXiv:1503.06834] [INSPIRE].

[32] M. Nemevšek, F. Nesti and J.C. Vasquez, *Majorana Higgses at colliders*, *JHEP* **04** (2017) 114 [arXiv:1612.06840] [INSPIRE].

[33] G. Senjanović and R.N. Mohapatra, *Exact Left-Right Symmetry and Spontaneous Violation of Parity*, *Phys. Rev. D* **12** (1975) 1502 [INSPIRE].

[34] F.I. Olness and M.E. Ebel, *Constraints on the Higgs Boson Masses in Left-right Electroweak Gauge Theories*, *Phys. Rev. D* **32** (1985) 1769 [INSPIRE].

JHEP06(2025)254

[35] J.F. Gunion et al., *Higgs Bosons in Left-Right Symmetric Models*, *Phys. Rev. D* **40** (1989) 1546 [INSPIRE].

[36] N.G. Deshpande, J.F. Gunion, B. Kayser and F.I. Olness, *Left-right symmetric electroweak models with triplet Higgs*, *Phys. Rev. D* **44** (1991) 837 [INSPIRE].

[37] K. Kiers, M. Assis and A.A. Petrov, *Higgs sector of the left-right model with explicit CP violation*, *Phys. Rev. D* **71** (2005) 115015 [hep-ph/0503115] [INSPIRE].

[38] A. Maiezza, G. Senjanović and J.C. Vasquez, *Higgs sector of the minimal left-right symmetric theory*, *Phys. Rev. D* **95** (2017) 095004 [arXiv:1612.09146] [INSPIRE].

[39] A. Maiezza, M. Nemevšek and F. Nesti, *Perturbativity and mass scales in the minimal left-right symmetric model*, *Phys. Rev. D* **94** (2016) 035008 [arXiv:1603.00360] [INSPIRE].

[40] G. Chauhan, P.S.B. Dev, R.N. Mohapatra and Y. Zhang, *Perturbativity constraints on $U(1)_{B-L}$ and left-right models and implications for heavy gauge boson searches*, *JHEP* **01** (2019) 208 [arXiv:1811.08789] [INSPIRE].

[41] R.N. Mohapatra, G. Yan and Y. Zhang, *Ameliorating Higgs induced flavor constraints on TeV scale W_R*, *Nucl. Phys. B* **948** (2019) 114764 [arXiv:1902.08601] [INSPIRE].

[42] N.D. Christensen and C. Duhr, *FeynRules — Feynman rules made easy*, *Comput. Phys. Commun.* **180** (2009) 1614 [arXiv:0806.4194] [INSPIRE].

[43] A. Alloul et al., *FeynRules 2.0 — A complete toolbox for tree-level phenomenology*, *Comput. Phys. Commun.* **185** (2014) 2250 [arXiv:1310.1921] [INSPIRE].

[44] C. Degrande et al., *UFO — The Universal FeynRules Output*, *Comput. Phys. Commun.* **183** (2012) 1201 [arXiv:1108.2040] [INSPIRE].

[45] L. Darmé et al., *UFO 2.0: the 'Universal Feynman Output' format*, *Eur. Phys. J. C* **83** (2023) 631 [arXiv:2304.09883] [INSPIRE].

[46] ATLAS collaboration, *Search for new resonances in mass distributions of jet pairs using 139 fb^{-1} of pp collisions at $\sqrt{s} = 13$ TeV with the ATLAS detector*, *JHEP* **03** (2020) 145 [arXiv:1910.08447] [INSPIRE].

[47] CMS collaboration, *Search for high mass dijet resonances with a new background prediction method in proton-proton collisions at $\sqrt{s} = 13$ TeV*, *JHEP* **05** (2020) 033 [arXiv:1911.03947] [INSPIRE].

[48] CMS collaboration, *Search for W' bosons decaying to a top and a bottom quark in leptonic final states in proton-proton collisions at $\sqrt{s} = 13$ TeV*, *JHEP* **05** (2024) 046 [arXiv:2310.19893] [INSPIRE].

[49] ATLAS collaboration, *Search for vector-boson resonances decaying into a top quark and a bottom quark using pp collisions at $\sqrt{s} = 13$ TeV with the ATLAS detector*, *JHEP* **12** (2023) 073 [arXiv:2308.08521] [INSPIRE].

[50] G. Senjanović and V. Tello, *Right Handed Quark Mixing in Left-Right Symmetric Theory*, *Phys. Rev. Lett.* **114** (2015) 071801 [arXiv:1408.3835] [INSPIRE].

[51] G. Senjanović and V. Tello, *Restoration of Parity and the Right-Handed Analog of the CKM Matrix*, *Phys. Rev. D* **94** (2016) 095023 [arXiv:1502.05704] [INSPIRE].

[52] W.-Y. Keung and G. Senjanović, *Majorana Neutrinos and the Production of the Right-handed Charged Gauge Boson*, *Phys. Rev. Lett.* **50** (1983) 1427 [INSPIRE].

[53] M. Frank et al., *A novel search strategy for right-handed charged gauge bosons at the Large Hadron Collider*, *JHEP* **02** (2024) 150 [arXiv:2312.08521] [INSPIRE].

JHEP06(2025)254

[54] M. Nemevšek, F. Nesti, G. Senjanović and Y. Zhang, *First Limits on Left-Right Symmetry Scale from LHC Data*, *Phys. Rev. D* **83** (2011) 115014 [arXiv:1103.1627] [INSPIRE].

[55] M. Mitra, R. Ruiz, D.J. Scott and M. Spannowsky, *Neutrino Jets from High-Mass W_R Gauge Bosons in TeV-Scale Left-Right Symmetric Models*, *Phys. Rev. D* **94** (2016) 095016 [arXiv:1607.03504] [INSPIRE].

[56] M. Nemevšek, F. Nesti and G. Popara, *Keung-Senjanović process at the LHC: From lepton number violation to displaced vertices to invisible decays*, *Phys. Rev. D* **97** (2018) 115018 [arXiv:1801.05813] [INSPIRE].

[57] CMS collaboration, *Search for new physics in the lepton plus missing transverse momentum final state in proton-proton collisions at $\sqrt{s} = 13$ TeV*, *JHEP* **07** (2022) 067 [arXiv:2202.06075] [INSPIRE].

[58] CMS collaboration, *Search for new physics in the τ lepton plus missing transverse momentum final state in proton-proton collisions at $\sqrt{s} = 13$ TeV*, *JHEP* **09** (2023) 051 [arXiv:2212.12604] [INSPIRE].

[59] ATLAS collaboration, *Search for a heavy charged boson in events with a charged lepton and missing transverse momentum from pp collisions at $\sqrt{s} = 13$ TeV with the ATLAS detector*, *Phys. Rev. D* **100** (2019) 052013 [arXiv:1906.05609] [INSPIRE].

[60] R. Ruiz, *Lepton Number Violation at Colliders from Kinematically Inaccessible Gauge Bosons*, *Eur. Phys. J. C* **77** (2017) 375 [arXiv:1703.04669] [INSPIRE].

[61] M. Nemevšek and F. Nesti, *Left-right symmetry at an FCC-hh*, *Phys. Rev. D* **108** (2023) 015030 [arXiv:2306.12104] [INSPIRE].

[62] P.S.B. Dev, D. Kim and R.N. Mohapatra, *Disambiguating Seesaw Models using Invariant Mass Variables at Hadron Colliders*, *JHEP* **01** (2016) 118 [arXiv:1510.04328] [INSPIRE].

[63] J. Gluza, T. Jelinski and R. Szafron, *Lepton number violation and 'Diracness' of massive neutrinos composed of Majorana states*, *Phys. Rev. D* **93** (2016) 113017 [arXiv:1604.01388] [INSPIRE].

[64] A. Das, N. Nagata and N. Okada, *Testing the "2 TeV Resonance with Trileptons*, *JHEP* **03** (2016) 049 [arXiv:1601.05079] [INSPIRE].

[65] A. Das, P.S.B. Dev and R.N. Mohapatra, *Same Sign versus Opposite Sign Dileptons as a Probe of Low Scale Seesaw Mechanisms*, *Phys. Rev. D* **97** (2018) 015018 [arXiv:1709.06553] [INSPIRE].

[66] J.C. Helo et al., *Probing neutrino Dirac mass in left-right symmetric models at the LHC and next generation colliders*, *Phys. Rev. D* **99** (2019) 055042 [arXiv:1812.01630] [INSPIRE].

[67] S. Dawson, P.P. Giardino and S. Homiller, *Uncovering the High Scale Higgs Singlet Model*, *Phys. Rev. D* **103** (2021) 075016 [arXiv:2102.02823] [INSPIRE].

[68] G. Senjanović and V. Tello, *Probing Seesaw with Parity Restoration*, *Phys. Rev. Lett.* **119** (2017) 201803 [arXiv:1612.05503] [INSPIRE].

[69] G. Senjanović and V. Tello, *Disentangling the seesaw mechanism in the minimal left-right symmetric model*, *Phys. Rev. D* **100** (2019) 115031 [arXiv:1812.03790] [INSPIRE].

[70] J. Kiers, K. Kiers, A. Szynkman and T. Tarutina, *Disentangling the seesaw mechanism in the left-right model: An algorithm for the general case*, *Phys. Rev. D* **107** (2023) 075001 [arXiv:2212.14837] [INSPIRE].

JHEP06(2025)254

[71] J. Alwall et al., *The automated computation of tree-level and next-to-leading order differential cross sections, and their matching to parton shower simulations*, *JHEP* **07** (2014) 079 [arXiv:1405.0301] [INSPIRE].

[72] H.H. Patel, *Package-X: A Mathematica package for the analytic calculation of one-loop integrals*, *Comput. Phys. Commun.* **197** (2015) 276 [arXiv:1503.01469] [INSPIRE].

[73] H.H. Patel, *Package-X 2.0: A Mathematica package for the analytic calculation of one-loop integrals*, *Comput. Phys. Commun.* **218** (2017) 66 [arXiv:1612.00009] [INSPIRE].

[74] T. Hahn and M. Perez-Victoria, *Automatized one loop calculations in four-dimensions and D-dimensions*, *Comput. Phys. Commun.* **118** (1999) 153 [hep-ph/9807565] [INSPIRE].

[75] NNPDF collaboration, *The path to proton structure at 1% accuracy*, *Eur. Phys. J. C* **82** (2022) 428 [arXiv:2109.02653] [INSPIRE].

[76] A. Buckley et al., *LHAPDF6: parton density access in the LHC precision era*, *Eur. Phys. J. C* **75** (2015) 132 [arXiv:1412.7420] [INSPIRE].

[77] P. Artoisenet, R. Frederix, O. Mattelaer and R. Rietkerk, *Automatic spin-entangled decays of heavy resonances in Monte Carlo simulations*, *JHEP* **03** (2013) 015 [arXiv:1212.3460] [INSPIRE].

[78] J. Alwall et al., *Computing decay rates for new physics theories with FeynRules and MadGraph 5_aMC@NLO*, *Comput. Phys. Commun.* **197** (2015) 312 [arXiv:1402.1178] [INSPIRE].

[79] C. Bierlich et al., *A comprehensive guide to the physics and usage of PYTHIA 8.3*, *SciPost Phys. Codeb.* **2022** (2022) 8 [arXiv:2203.11601] [INSPIRE].

[80] E. Conte, B. Fuks and G. Serret, *MadAnalysis 5, A User-Friendly Framework for Collider Phenomenology*, *Comput. Phys. Commun.* **184** (2013) 222 [arXiv:1206.1599] [INSPIRE].

[81] E. Conte, B. Dumont, B. Fuks and C. Wymant, *Designing and recasting LHC analyses with MadAnalysis 5*, *Eur. Phys. J. C* **74** (2014) 3103 [arXiv:1405.3982] [INSPIRE].

[82] E. Conte and B. Fuks, *Confronting new physics theories to LHC data with MADANALYSIS 5*, *Int. J. Mod. Phys. A* **33** (2018) 1830027 [arXiv:1808.00480] [INSPIRE].

[83] J.Y. Araz, B. Fuks, M.D. Goodsell and M. Utsch, *Recasting LHC searches for long-lived particles with MadAnalysis 5*, *Eur. Phys. J. C* **82** (2022) 597 [arXiv:2112.05163] [INSPIRE].

[84] CMS collaboration, *Search for a right-handed W boson and a heavy neutrino in proton-proton collisions at* $\sqrt{s} = 13$ *TeV*, *JHEP* **04** (2022) 047 [arXiv:2112.03949] [INSPIRE].

[85] ATLAS collaboration, *Search for heavy Majorana or Dirac neutrinos and right-handed W gauge bosons in final states with charged leptons and jets in pp collisions at* $\sqrt{s} = 13$ *TeV with the ATLAS detector*, *Eur. Phys. J. C* **83** (2023) 1164 [arXiv:2304.09553] [INSPIRE].

[86] DELPHES 3 collaboration, *DELPHES 3, A modular framework for fast simulation of a generic collider experiment*, *JHEP* **02** (2014) 057 [arXiv:1307.6346] [INSPIRE].

[87] M. Cacciari, G.P. Salam and G. Soyez, *The anti-k_t jet clustering algorithm*, *JHEP* **04** (2008) 063 [arXiv:0802.1189] [INSPIRE].

[88] M. Cacciari, G.P. Salam and G. Soyez, *FastJet User Manual*, *Eur. Phys. J. C* **72** (2012) 1896 [arXiv:1111.6097] [INSPIRE].

[89] ATLAS collaboration, *Electron and photon efficiencies in LHC Run 2 with the ATLAS experiment*, *JHEP* **05** (2024) 162 [arXiv:2308.13362] [INSPIRE].

JHEP06(2025)254

[90] J.Y. Araz, B. Fuks and G. Polykratis, *Simplified fast detector simulation in MADANALYSIS 5*, *Eur. Phys. J. C* **81** (2021) 329 [arXiv:2006.09387] [INSPIRE].

[91] J.Y. Araz, A. Buckley and B. Fuks, *Searches for new physics with boosted top quarks in the MadAnalysis 5 and Rivet frameworks*, *Eur. Phys. J. C* **83** (2023) 664 [arXiv:2303.03427] [INSPIRE].

[92] ATLAS collaboration, *Performance of the reconstruction of large impact parameter tracks in the inner detector of ATLAS*, *Eur. Phys. J. C* **83** (2023) 1081 [arXiv:2304.12867] [INSPIRE].

[93] ATLAS collaboration, *Search for displaced vertices of oppositely charged leptons from decays of long-lived particles in pp collisions at* $\sqrt{s} = 13$ *TeV with the ATLAS detector*, *Phys. Lett. B* **801** (2020) 135114 [arXiv:1907.10037] [INSPIRE].

[94] J. Heeck and W. Rodejohann, *Neutrinoless Quadruple Beta Decay*, *EPL* **103** (2013) 32001 [arXiv:1306.0580] [INSPIRE].

[95] A.S. Barabash, P. Hubert, A. Nachab and V.I. Umatov, *Search for triple and quadruple* β *decay of* ^{150}Nd, *Phys. Rev. C* **100** (2019) 045502 [arXiv:1906.07180] [INSPIRE].

[96] G.P. Lepage, *A New Algorithm for Adaptive Multidimensional Integration*, *J. Comput. Phys.* **27** (1978) 192 [INSPIRE].

[97] G.P. Lepage, *Adaptive multidimensional integration: VEGAS enhanced*, *J. Comput. Phys.* **439** (2021) 110386 [arXiv:2009.05112] [INSPIRE].

[98] Particle Data Group collaboration, *Review of particle physics*, *Phys. Rev. D* **110** (2024) 030001 [INSPIRE].

JHEP06(2025)254